pubs.acs.org/Biomac

Article

Dual Functionalized Injectable Hybrid Extracellular Matrix Hydrogel for Burn Wounds

Kamakshi Bankoti, Arun Prabhu Rameshbabu, Sayanti Datta, Piyali Goswami, Madhurima Roy, Dipankar Das, Sudip Kumar Ghosh, Amit Kumar Das, Analava Mitra, Sagar Pal, Dhrubajyoti Maulik, Bo Su, Paulomi Ghosh, Bikramajit Basu, and Santanu Dhara*

Cite This: *Biomacromolecules* 2021, 22, 514–533

Read Online

ACCESS | Metrics & More | Article Recommendations | Supporting Information

ABSTRACT: Low strength and rapid biodegradability of acellular dermal matrix (ADM) restrict its wider clinical application as a rapid cell delivery platform *in situ* for management of burn wounds. Herein, the extracted ADM was modified by a dual cross-linking approach with ionic crosslinking using chitosan and covalent cross-linking using an iodine-modified 2,5-dihydro-2,5-dimethoxy-furan cross-linker, termed as CsADM-Cl. In addition, inherent growth factors and cytokines were found to be preserved in CsADM-Cl, irrespective of ionic/covalent crosslinking. CsADM-Cl demonstrated improvement in post crosslinking stiffness with a decreased biodegradation rate. This hybrid crosslinked hydrogel supported adhesion, proliferation, and migration of human foreskin-derived fibroblasts and keratinocytes. Also, the angiogenic potential of CsADM-Cl was manifested by chick chorioallantoic membrane assay. CsADM-Cl showed excellent antibacterial activity against *Escherichia coli* and *Staphylococcus aureus*. Moreover, CsADM-Cl treated full thickness burn wounds and demonstrated rapid healing marked with superior angiogenesis, well-defined dermal–epidermal junctions, mature basket weave collagen deposition, and development of more pronounced secondary appendages. Altogether, the bioactive CsADM-Cl hydrogel established significant clinical potential to support wound healing as an apt injectable antibacterial matrix to encounter unmet challenges concerning critical burn wounds.

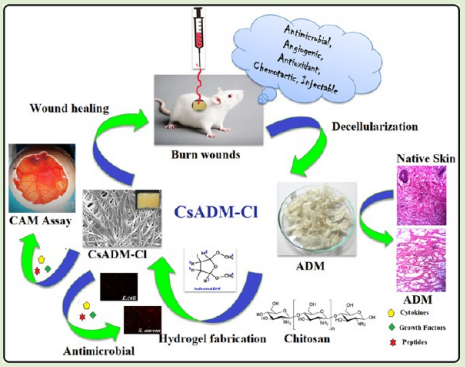

1. INTRODUCTION

Burn injuries, a multifaceted acute wound, represent complex inflammatory progression, that is, intense local inflammation marked by a pronounced propensity to infections. Especially, full thickness (FT) wounds of critical size (diameter >1 cm), induced by burn, result in rapid loss of liquid and also curtail various vital functions of the skin, leading to the development of chronic wounds. Hence, these critical wounds are prone to complications, such as secondary necrosis.[1] Further, healing progression is impeded by restricted blood flow and complex inflammatory reactions, which are stimulated by an initial burn injury.[2] To add up to this slowed down regeneration, these wounds are susceptible to microbial infections and lead to scarring upon healing, thus complicating the treatment modalities.[3]

Hydrogels with *in situ* gelation property are preferred as a skin substitute for burn wound management due to their minimal invasiveness and ability to fill the irregular tissue defects. Hydrogels are capable of lending a moist environment that accelerates cell proliferation and collagen deposition in the wound bed along with the delivery of bioactive target molecules.[4,5] Bioactive molecules like hormones, cytokines, growth factors, and peptides are reported to promote healing progression. However, their high cost of production limits their application.[6,7] Also, hydrogels with antibacterial activity are widely explored, either by encapsulating antibacterial molecules into the hydrogel or self-assembling alternate Lys–Val peptides. However, the former causes burst release of antibiotics, whereas in case of latter, the high cost of production, complex preparation protocol, and poor tenability limit their application.[8,9] Iodine is reported to exhibit broad-spectrum antimicrobial properties and hence is being used frequently in clinics as an antiseptic and antimicrobial agent.[10] Notably, the potential of bacterial resistance is significantly reduced due to the alternative mechanism of antimicrobial activity of iodine.[11] For instance, iodine conjugated with polyvinylpyrrolidone known as povidone-iodine has been demonstrated to exhibit antimicrobial property, even against methicillin-resistant strains.[12] Altogether, there is an urgent clinical need to develop simple techniques to tackle the stringent pathophysiological requirements of chronic injuries

Received: September 28, 2020
Revised: November 20, 2020
Published: December 8, 2020

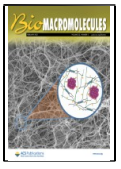

https://dx.doi.org/10.1021/acs.biomac.0c01400
Biomacromolecules 2021, 22, 514–533

to induce rapid wound closure and to minimize scar development.

Chitosan (CTS) dressings have been used widely for wound healing purposes owing to their excellent biocompatibility, biodegradability, antibacterial property, hemostatic nature, and also for drug/biomolecule delivery.[13,14] CTS resembles glycoaminoglycan (GAGs) in structure; however, CTS lacks bioactive signals equivalent to those existing in the extracellular matrix (ECM) for cell attachment, growth, and differentiation. The decoration of cytokines, growth factors, signaling molecules, proteins, or small cell-binding peptides onto the polymer surface is used as a strategy to enhance as well as to direct cell responses on biomaterial surfaces.[15−20] In comparison to synthetic matrices that fail to mimic the complexity of the ECM *in vivo*, biological scaffolds composed of the decellularized ECM (dECM) embody structures akin to the host tissue with superior properties such as a natural 3D morphology, RGDs promoting cell adhesion and proliferation, and inherent biodegradability. The dECM has been reported to have potential to guide cell differentiation into appropriate tissue type structures and phenotype.[21−23] Further, the dECM supports *in vivo* tissue remodeling and regeneration. Also, ECM degradation products act as a chemoattractant for the recruitment of endogenous stem and progenitor cells and modulates innate immune response.[24,25] dECM scaffolds from various species and tissue have been approved by FDA and are being used clinically for soft tissue repair, wound management, or heart valve replacement.[26,27] However, decellularized scaffolds may restrict its application due to irregular contours of a wound bed. Thus, *in situ* gelling hydrogels of the pepsin-digested dECM will be of great importance. pH-sensitive *in vivo* gelling hydrogels of the ECM have been characterized for the preservation of biomolecules in an intact form.[28,29] Also, the hybrid dECM has been explored for preparing scaffolds, hydrogels, nanofibers, and microspheres.[30−33] However, the dECM has weak mechanical strength and poor biostability and is prone to microbial contamination. Therefore, its use for cell encapsulation and wound healing is questionable. To this end, crosslinking of the ECM is being explored in this work. A cross-linking reaction can be performed using chemical reagents (like glutaraldehydes, carbodiimide, and genipin), UV light, and enzyme catalysis (such as transglutaminase).[34] Developing bioactive hydrogel with inherent antibacterial activity is a fascinating challenge for the clinical management of burn wounds.

To address this challenge, we have developed injectable soluble acellular dermal matrix (sADM)-based hybrid hydrogel platforms based on double crosslinks—forming ionic and covalent bonds for facilitating the recovery of critical FT thermal burn injury in a rat model. A process to dissolve ADM was developed, and hybrid crosslinked hydrogel (CsADM-Cl) was formed by blending with CTS, a natural linear biocompatible polysaccharide, and iodine-modified 2,5-dihydro-2,5-dimethoxy-furan (DHF-I), a covalent crosslinker. To the best of our knowledge, there is no report of crosslinking ADM using DHF-I, which not only preserves the ECM biological composition and ultrastructure but also enhances its mechanical strength and control the biodegradation rate as well as provides the unique antibacterial and antioxidant property to the gel. Collagen (Col), being the major protein in the dermal matrix, has been explored for its efficacy in wound healing models, and therefore, it was selected as a control for the study. Fabricated hydrogels were characterized for their physio-mechanical attributes and subsequently assessed for cytocompatibility using human foreskin-derived fibroblasts (HFCs) and keratinocytes (HKC). Wound healing and angiogenic potential of hydrogels were evaluated *in vitro* using scratch and chick chorioallantoic membrane (CAM) assay. Wound regeneration was analyzed through histological observations, marker protein expressions, and immunostaining of the wound tissue across days of recovery. Furthermore, neo-blood vessel formation, collagen organization, and skin appendage formation were determined to evaluate the effect of bioactive cross-linked hybrid hydrogel treatment in the wound repair process.

2. EXPERIMENTAL SECTION

2.1. Decellularization of Skin Tissue. Decellularization of the skin was carried out using a modified protocol described elsewhere.[35,36] FT skin was harvested from adult rats (weighing ∼150−200 g) and preserved in cold phosphate buffer saline (PBS) containing 0.1% gentamycin, followed by washing several times using PBS to remove the adhered blood. Samples were processed within 4 h from harvesting. Dermal hair and epidermis were removed using a hypertonic solution (4 g of sodium chloride, 605 mg of tris base, and 202.5 mg of EDTA in 100 mL PBS) for 2−4 h in an orbital shaker (Thermocon Instruments Private Limited, Bangalore, India) and maintained at 37 °C. The isolated dermal layer was denuded using trypsin (0.25%, Thermo Fisher Scientific, USA) and Triton X-100 (Sigma-Aldrich, USA, 0.5% v/v) treatments and washed several times using PBS. The ADM was further treated with a fat digestion solution (chloroform/methanol—1:1 v/v) for 2 h and subsequently washed with sterile PBS thoroughly and stored at −80 °C. Frozen ADM was lyophilized and pulverized mechanically at 4 °C. A pulverized ADM was solubilized enzymatically (acidic pepsin solution 1 mg/mL) to form a sADM and stored at −80 °C until required. The ADM was characterized by staining with hematoxylin and eosin (H&E), anti-Col I antibody (Col I), alcian blue (AB), DAPI, and DNA quantification, following the protocol described in the Supporting Information. To investigate the retained proteins after decellularization, the native skin (NS) and ADM were assessed by sodium dodecyl sulphate-polyacrylamide gel electrophoresis (SDS-PAGE) as detailed in the Supporting Information. Further, sGAGs and Col were also quantified using colorimetric assays (detailed in Supporting Information). The tissue homogenate prepared aforesaid was analyzed using ELISA Kits (Invitrogen, USA) to investigate the presence of the growth factors [BMP-2, vascular endothelial growth factor (VEGF), and transforming growth factor-β (TGF-β)]. Samples were run in triplicate; averaged and standard curve was used to measure the concentrations of growth factors in the NS and ADM.

For Col isolation, rat tail was harvested from freshly euthanized adult albino rats (average weight 150−200 g) using a protocol described elsewhere.[37] Briefly, the tail was washed with PBS to remove the adherent dirt, and the epidermis was removed mechanically using a surgical blade and tweezers. Col fibers from rat tail tendon were cut to smaller fragments and washed successively with acetone and 70% v/v isopropanol. Rinsed fibers were dissolved in acetic acid (0.02 N) for 48 h at 4 °C and dialyzed against 1% chloroform water for 1 h and then changed to water for 2 days to remove acetic acid. Col solution was lyophilized after freezing and further stored at −80 °C, until use. Col was characterized using SDS PAGE (details in Supporting Information).

2.2. Synthesis of Iodine-Modified DHF-I. DHF-I was synthesized as described elsewhere.[38] Iodine was dissolved in 20% v/v ethanol and mixed with DHF (15%) at 25 °C. The reaction was allowed to complete in an acidic environment for 12 h until reaction color changes from reddish brown to yellow. Subsequently, pH 7 was maintained using sodium hydroxide (NaOH) solution. The product was filtered to remove the precipitate, if any. The iodination of DHF was confirmed by proton nuclear magnetic resonance spectroscopy (400 MHz, Advance DAX-400 Bruker, Sweden) using deuterium

https://dx.doi.org/10.1021/acs.biomac.0c01400
Biomacromolecules 2021, 22, 514−533

oxide (Sigma-Aldrich, USA) as a solvent, and the spectrum was compared with the spectrum of pristine DHF.

2.3. Preparation of Hybrid Hydrogel. CCol-Cl and CsADM-Cl hydrogels were prepared by blending CTS (molecular weight 50,000−190,000 Da; 75−85% deacetylated, Sigma-Aldrich, USA) and Col/sADM using DHF-I as a crosslinker. In brief, the blend was neutralized using 0.1 M NaOH in 10× PBS buffer in ice (to maintain temperature 0−10 °C), such that the final concentration of the polymer and protein in the gel would be 8 mg/mL each and PBS will become 1×. Further, pregel solution was crosslinked using 0.5% DHF-I, forming a rapid hydrogel. Crosslinked hydrogels were denoted as CCol-Cl and CsADM-Cl, while uncrosslinked hydrogels (without DHF-I) were designated as CCol and CsADM. Tube inversion method was used for measuring gelation time. Also, the pregel, not flowing for more than 30 s, was taken as a hydrogel. Surface topology of the hydrogels was observed using SEM, and fiber networks were analyzed using ImageJ (version 6). Further iodine distribution in the crosslinked matrix were confirmed by EDAX mapping of iodine on CCol-Cl/CsADM-Cl hydrogel. In brief, the hydrogels were coated on coverslips and kept at 37 °C for 15 min to facilitate gelation. Coated coverslips were dried in a desiccator and stored therein until SEM analysis was carried out after gold coating of the sample to avoid moisture.

2.4. Immunohistochemistry of Hydrogel. To assess the retention of important matrix proteins and biomolecules after crosslinking, immunohistochemistry (IHC) was performed on NS, ADM, CsADM, and CsADM-Cl. The primary antibodies against Col-I (Abcam), fibronectin, VEGF, TGF-β, interleukin-8 (IL-8), and monocyte chemoattractant protein-1 (MCP-1) (all Santa Cruz Biotechnology, Inc.) were used. The stained samples were imaged under an inverted fluorescent microscope (AxioVision, Zeiss, Germany).

2.5. Rheological Characterization. CCol, CsADM, CCol-Cl, and CsADM-Cl were further characterized for gelation kinetics using a dynamic shear rheometer (DSR+, Malvern, U.K.). Pregel solution was formed by blending CTS with Col/sADM. Gelation kinetics was assessed by a rheometer using parallel plate geometry; a gap of 200 μm and parallel plate of 25 mm were maintained in all the experiments. Pregel solution was neutralized in ice and loaded immediately to a pre-cooled rheology plate at 15 °C. Mineral oil was used to reduce evaporation from the edges, and the temperature was raised to 37 °C to induce gelation. Gelation kinetics was studied by applying constant frequency (1 Hz) and strain (0.1%). Further, the hydrogels were subjected to small oscillatory frequency sweep at strain 0.5% and frequency 0.5−20 Hz.

2.6. Fourier Transformer Infrared. Fourier transformer infrared (FTIR) spectroscopy of the hydrogels was performed in ATR mode in the wavelength range of 500−4000 cm^{-1} on a Thermo Nicolet Spectrophotometer (model NEXUS-870; Thermo Nicolet Corporation, Madison, WI). Vacuum-dried hydrogels (CCol, CsADM, CCol-Cl and CsADM-Cl) were stored carefully in desiccators to avoid moisture, before FTIR spectra were recorded.

2.7. Iodine Dynamic Release Kinetics. To study the iodine dynamic release from cross-linked variant CsADM-Cl, hydrogel was incubated in PBS and buffered enzymatic solution (Collagenase I, Sigma, USA) to imitate *in vivo* conditions. The supernatant was collected at a predetermined period, that is, 2, 4, 6, 12, 24, 48, 72, and 96 h. In brief, 1 mL of pregel solution was gelled for 24 h in 37 °C, and the hydrogel was incubated with 10 mL of PBS/collagenase I (125 U/mL) in 0.1 M Tris base and 0.25 M $CaCl_2$ with pH maintained at 7.4 in 37 °C in an incubator and stirred using a mechanical stirrer at 100 rpm (schematic representation in Figure S4). At a predetermined period, 400 μL of supernatant was extracted from the sample vial and replenished with 400 μL of fresh PBS/buffered enzymatic solution to maintain a constant volume. Samples were centrifuged, and the collected supernatant was filtered through 0.2 μm syringe filter and stored at −80 °C until analyzed using Dionex ICS 2100 (Thermo Scientific, USA).

2.8. Antioxidant Efficiency of Hydrogels. The *ex vivo* antioxidant efficacy of CCol-Cl and CsADM-Cl was assessed by measuring their potential to scavenge the stable 1,1-diphenyl-2-picrylhydrazyl (DPPH, Sigma-Aldrich, USA) free radical, following the protocol described elsewhere with minor modifications.[39] The uncrosslinked/crosslinked hydrogels were homogenized to powder using liquid nitrogen. Briefly, DPPH (3.0 mL, 100 μM) and dispersion of samples (containing 5 mg) in methanol were stirred and incubated in a dark place for 30 min. Then, DPPH scavenging was assessed by measuring the absorbance using a UV−vis spectrophotometer (Multiskan GO Microplate Spectrophotometer, Thermo Fisher Scientific, USA) at 517 nm and calculated using the following equation

$$\text{DPPH scavenging \%} = \frac{A_B - A_H}{A_B} \times 100$$

where A_B is the absorption of the blank (DPPH in methanol) and A_H the absorption of the hydrogel (hydrogel with DPPH in methanol). Samples were run in triplicate and averaged.

2.9. Hemocompatibility. The hemocompatible characteristics of the hydrogels was evaluated using the heparinized blood, following a protocol described elsewhere.[40] Heparinized blood was centrifuged to obtain RBC pellets, and the pellet was subsequently washed thrice with (4-(2-hydroxyethyl)-1-piperazine ethane sulfonic acid) (5 mM) buffer containing sodium chloride (150 mM). To hydrogels/normal saline (negative control)/1% Triton X-100 (positive control), 200 μL of the suspension (5% diluted anticoagulant blood solution in 0.9% NaCl solution) was added and further incubated for 30 min at 37 °C. The supernatant was collected post-centrifugation (1000*g*, 10 min), and the absorbance was recorded at 540 nm (n = 3).

The % hemolysis was evaluated using the following equation

$$\text{Hemolysis (\%)} = \frac{A_s - A_{NC}}{A_{PC} - A_{NC}} \times 100$$

where A_s is the absorption of the sample, A_{PC} is absorbance of positive control, and A_{NC} is the absorption of negative control.

2.10. Bacterial Inhibition. The hydrogels were prepared in sterile 24-well plates and washed with sterile PBS to ensure sterility of the samples before analyzing antibacterial efficacy.[41] *Staphylococcus aureus* (N315) and *Escherichia coli* (DH5α) strains were taken for the present study. 20 μL of bacterial suspensions (5×10^7 cfu mL^{-1}) was spread onto each hydrogel (CCol, CsADM, CCol-Cl, and CsADM-Cl) in a tissue culture plate (TCP) and incubated for 2 h at 37 °C, relative humidity >90%. To collect bacterial survivors, post 2 h treatment, sterile PBS (1 mL) was added, and a series of 10-fold dilution was prepared, followed by plating out in Luria Bertani agar. Survivor bacteria were allowed to grow for 16−18 h by incubating at 35 °C and counted for colony-forming units (cfu). The TCP served as a control and was processed in a similar fashion like other samples. The results are expressed as

$$\text{Log Reduction (\%)} = \frac{C_c - C_H}{C_c} \times 100$$

where C_c is log (cell count of control), and C_H is survivor count on hydrogel.

For Live/Dead assay, the chosen bacterial strains were seeded on hydrogels as aforesaid, and post-incubation, the nutrient broth was removed. Subsequently, the hydrogels were washed with PBS, Live/Dead solution (3 μg/mL ethidium bromide and 5 μg/mL acridine orange in PBS) was added to each hydrogel, and the plates were incubated at 37 °C for 15 min in the dark. After this, the samples were washed with PBS and imaged using a Carl Zeiss fluorescence microscope. The experiment was repeated twice in triplicate, and the data represent average with standard deviation (SD).

2.11. CAM Assay. The angiogenic potential of the hydrogel (CCol-Cl and CsADM-Cl) was investigated by CAM assay, following a protocol reported earlier.[33] Fertilized chicken eggs procured (regional poultry farm, Midnapore, West Bengal, India) were cleaned with warm sterile saline, wiped, and incubated at 37 °C, 60% humidity. After 3 days, sterilized hydrogels (CCol-Cl and CsADM-Cl) were implanted onto the CAM of the eggs with careful sterile

https://dx.doi.org/10.1021/acs.biomac.0c01400
Biomacromolecules 2021, 22, 514−533

dissection, making a small window away from the embryo (n = 3). The window was resealed through adhesive tape, and the eggs were further incubated until day 8 of embryo development. Post-incubation period, the hydrogel-treated CAM membrane was photographed and analyzed for angiogenesis. The vessels approaching toward the scaffold was counted by three independent observers, and results were reported by taking the average.

2.12. Cell Culture Study. *2.12.1. Conditioning Media and Related Assays.* The matricryptic peptides or cytokines, a major portion of eluted components, may affect scaffold cellularization and remodeling. All materials were processed under sterile conditions in a blinded fashion. Each hydrogel was weighed equally and minced using a sterile razor; subsequently, minced hydrogels were placed in six-well plates. Dulbecco's minimum essential medium high glucose (Life Technologies, USA) was added to minced hydrogels (ratio: 50 mg hydrogel/mL medium) and incubated at 37 °C, 5% CO_2. Untreated medium was processed simultaneously and acted as a control for the study. 72 h post incubation, the media was centrifuged (16,000g for 10 min) for removing hydrogel particles, and the untreated medium was added to attain a final concentration of 25 mg crushed hydrogel/mL medium. The morphological changes of HFCs/HKCs was documented using rhodamine and DAPI (Invitrogen, Thermo Scientific, USA) staining.[42] 15,000 cells/coverslip were seeded and cultivated for a predetermined period, that is, 72 h. Post the preset period, cells were fixed using 4% paraformaldehyde (PFA) and stained for rhodamine & DAPI, and images were recorded using a fluorescence microscope (Carl Zeiss) for evaluating cytocompatibility of different hydrogel's conditioned media, where the complete media acted as a control for the study.

The conditioning media was also subjected to scratch assay using HFCs/HKCs to study the role of conditioning media in supporting the migration potential of HFCs/HKCs. Scratch assay was performed to evaluate *in vitro* wound healing potential of the conditioning media of the hydrogel. In brief, HFCs were grown until the formation of the monolayer; then wound/scratch was created using a sterile 200 μm tip. The plates were washed carefully twice with sterile PBS to remove any unattached cells on the plate and wound area. The complete media was replaced with the conditioning media, and micrographs were obtained after a predetermined period (*i.e.* HFC—6 and 12 h; HKC—12 and 24 h). The number of migrated cells in denuded area was also calculated for both HFCs and HKCs by three independent observers, and the results were demonstrated as mean ± SD.

2.12.2. Direct Cytotoxicity Testing. 2.12.2.1. MTT Assay. The cytotoxicity of hydrogels was evaluated using 3-(4,5-dimethyl-2-thiazolyl)-2,5-diphenyl-2*H*-tetrazolium bromide (MTT) assay by directly cultivating HFCs/HKCs on CCol, CsADM, CCol-Cl, and CsADM-Cl. Viable cells were calculated at a predetermined (24, 72, and 120 h) period by incubating the hydrogel-coated coverslips with an MTT (Merk Millipore, Germany) solution and subsequently dissolving the formazan crystal by adding an equivalent amount of dimethyl sulfoxide. Subsequently, absorbance was taken at 570 nm, experiments were repeated thrice, and mean was taken.

2.12.2.2. Proliferation Assay. Proliferating cell nuclear antigen (PCNA) antibody (BioLegend, USA) was used for the immunofluorescent study (IF) of PCNA (green) in proliferating HFCs on hydrogels. Hydrogel-coated coverslips were seeded with HFCs (15,000 cells/coverslip) and incubated for 5 days. Post incubation, coverslips were fixed and permeabilized with ice-cold 70% ethanol for 15 min, followed by washing with PBS and blocking in BSA (1% in PBS) for 15 min at room temperature. Cells seeded with hydrogels were stained with PCNA monoclonal antibody tagged with secondary for 1 h at room temperature and subsequently washed with PBS to remove background and imaged using an inverted fluorescence microscope. The experiment was repeated thrice to confirm the reproducibility of data.

2.12.2.3. Apoptosis Assay. Apoptosis assay was executed using a DeadEnd Fluorometric Terminal deoxynucleotidyl transferase dUTP nick end labeling system (Promega, USA) following the manufacturer's guidelines. Briefly, hydrogel-coated coverslips were taken as the sample, and lysine-coated coverslips served as the control. HFCs were seeded (15,000 cells/coverslip) and cultivated for 5 days. Post 5 days of cultivation, samples were stained after processing, and images were documented using a ZEISS inverted fluorescence microscope.

2.12.3. Cells Encapsulation in Pre-Gel. For encapsulating HFCs in hydrogel, CCol-Cl and CsADM-Cl were processed in a sterile parallel blinded fashion. Gels were fabricated in 24-well plates containing 2 mL of pregel solution of each group with 1,00,000 HFCs/mL. After gelling, media was supplied to gels, and media was changed every day to avoid cell death. The viability of HFCs in hydrogels was determined post 72 h using the Live/Dead kit (Invitrogen, USA), following manufacturer's protocol. Labeled cells were then micrographed under an inverted microscope, and images were captured using the Zen software. Viable/Live cells were stained green (tagged with calcein AM), while dead cells were stained red (tagged with EthD-1).

2.12.4. Quantification of Hydrogel Contraction. CCol, CsADM, CCOl-Cl, and CsADM-Cl contraction after cells seeding/unseeded was analyzed using macroscopic image analysis (from two independent batches of ADM isolation). Free-floating crosslinked and uncrosslinked hydrogels were imaged after 12 h, 1, 3, and 7 days in culture.

2.13. Host Response of CCol-Cl and CsADM-Cl *In Vivo*. All *in vivo* experiments were executed under compliance of the Institutional Animal Ethical Committee guidelines of the Indian Institute of Technology, Kharagpur, India. To assess the host response *in vivo*, the subcutaneous injection of CCol-Cl and CsADM-Cl in the dorsal region was performed in albino Wistar rats (150−200 kg; n = 3 per group). Prior to the experiment, peritoneal injection of ketamine was performed to anesthetize the rats. Food and water supply were provided freely to the rats post-surgery 12 h, and the light/dark cycle of 12 h was maintained during the study. On day 14, the rats were sacrificed; CCol-Cl and CsADM-Cl along with surrounding tissues were retrieved, followed by fixation in 4% PFA and processed for H&E, TB, and Masson's trichome (MT) staining. Major organs were also harvested from rat on day 14 to assess organ toxicity, and H&E was performed to establish the biocompatibility of the hydrogels.

2.14. FT Wound Healing in Burn Model. *2.14.1. In Vivo Burn Model Creation.* For burn model, Wistar rats (150−200 g each) were taken, and all *in vivo* experiments were performed as per guidelines of the Institutional Animal Ethical Committee, Indian Institute of Technology, Kharagpur, India. Rats were anesthetized by intraperitoneal injection of ketamine hydrochloride; then their dorsum was shaved to remove hair. The burn model was created as previously reported.[43] Briefly, a custom-made 220 g aluminum rod with a copper template of 1.5 cm diameter was heated in a 100 °C water bath for 5 min and placed on the posterior-dorsum of each rat for 8 s. Subsequently, the rat was resuscitated by intraperitoneal injection of saline within 1 h post burning. To follow the current clinically accepted treatment, burn wound excisions were executed 48 h post burn injury. The FT skin was removed to generate a 2 cm diameter circular wound; CCol-Cl/CsADM-Cl pregel was injected at the wound site, and Tegaderm dressing (3M Science Applied to Life, USA) was applied to hydrogels on the wound bed. SHAM wounds were only covered with Tegaderm dressing. For the study, three rats were taken for each group and for each period.

2.14.2. Histomorphometric Analysis. Hydrogel explants were collected at days 7, 14, and 21 and fixed using 4% PFA. Following fixation, tissues were dehydrated in ethanol graded series (70−100%), embedded in paraffin to form a block, sectioned using a microtome (3 μm thickness), and stained with H&E. Section images were processed using ImageJ (version 6) for quantification of re-epithelialization, wound distance, granulation area, newly formed appendages, and thickness of the newly formed epithelium. MT staining was performed for the analysis of collagen morphology and intensity. Sections were also stained with anti-CD31 and anti-CK10 for confirmation of blood vessels and re-epithelialization in different groups.

2.15. Gene Expression (RT-PCR Analysis). Regenerated tissues were retrieved on day 21 from each group, and TRIzol Reagent (Thermo Scientific, USA) was used for isolation of total RNA following the manufacturer's instructions. RNA quality was

https://dx.doi.org/10.1021/acs.biomac.0c01400
Biomacromolecules 2021, 22, 514−533

Scheme 1. Synthesis Strategy of Crosslinked Hybrid Hydrogel[a]

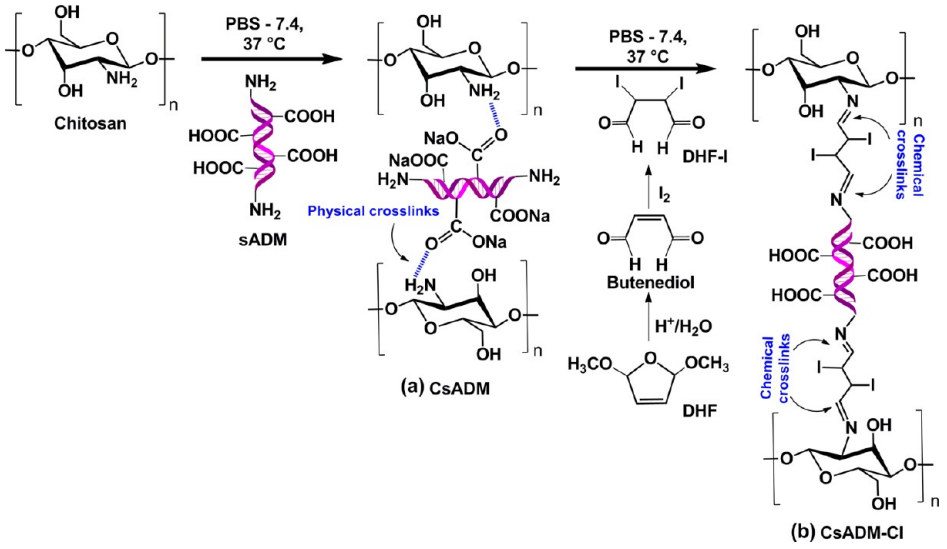

[a]Schematic representation of physical cross-linking between CTS and ADM at specific conditions to form hydrogel CsADM (a); further, CsADM was cross-linked using DHF-I to form CsADM-Cl (b).

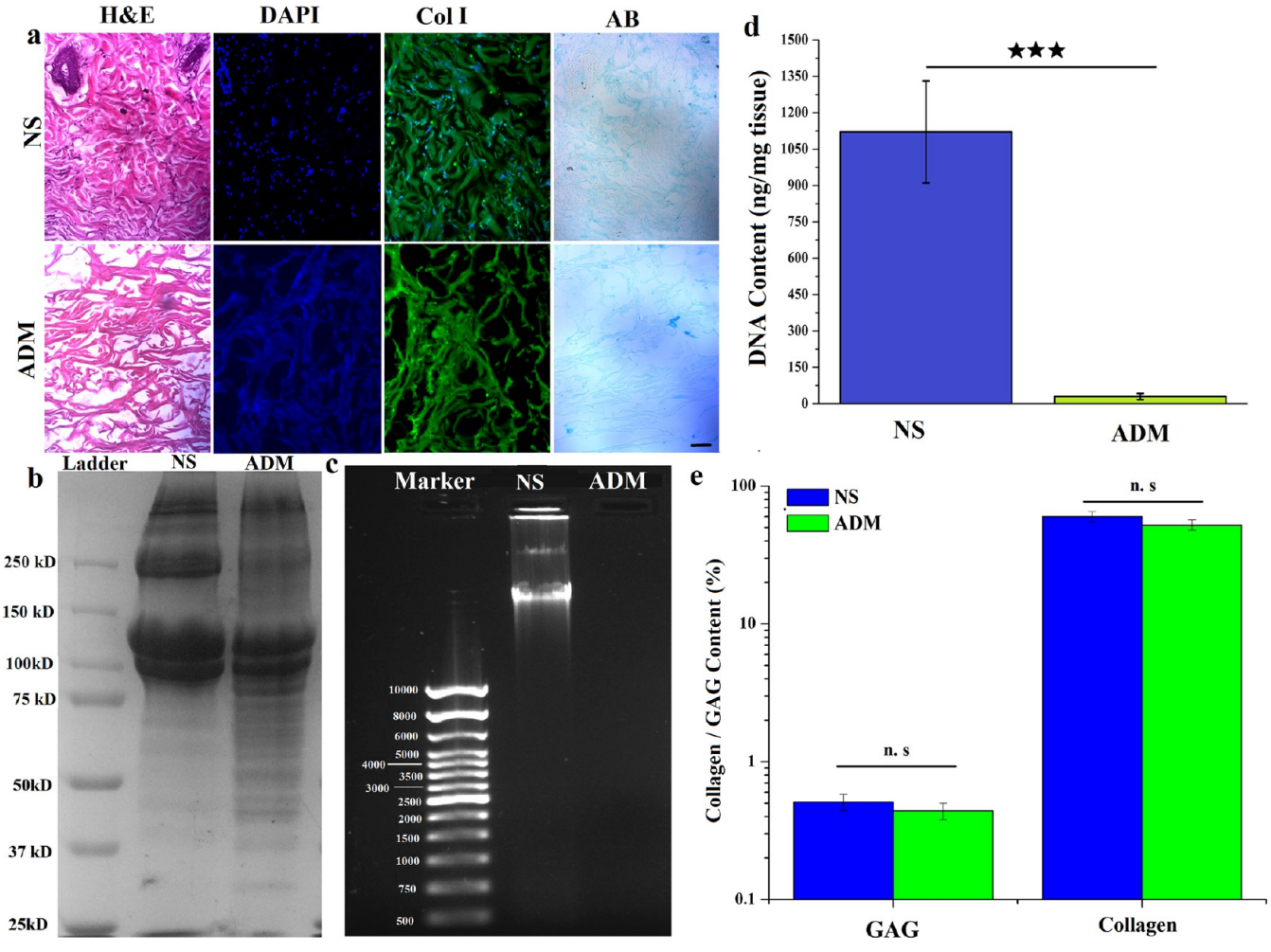

Figure 1. Decellularized skin was used as an ADM in developing a crosslinked hydrogel. Histological and immunohistochemical analysis of NS and ADM (a), total protein extracted from NS and ADM separated by SDS-PAGE (b), DNA isolation and quantification from NS and ADM (c,d), and quantification of GAGs and collagen from NS and ADM (e). Scale bar represents 50 μm, *Y*-error bars symbolize SD, and *** signifies $p < 0.001$.

https://dx.doi.org/10.1021/acs.biomac.0c01400
Biomacromolecules 2021, 22, 514−533

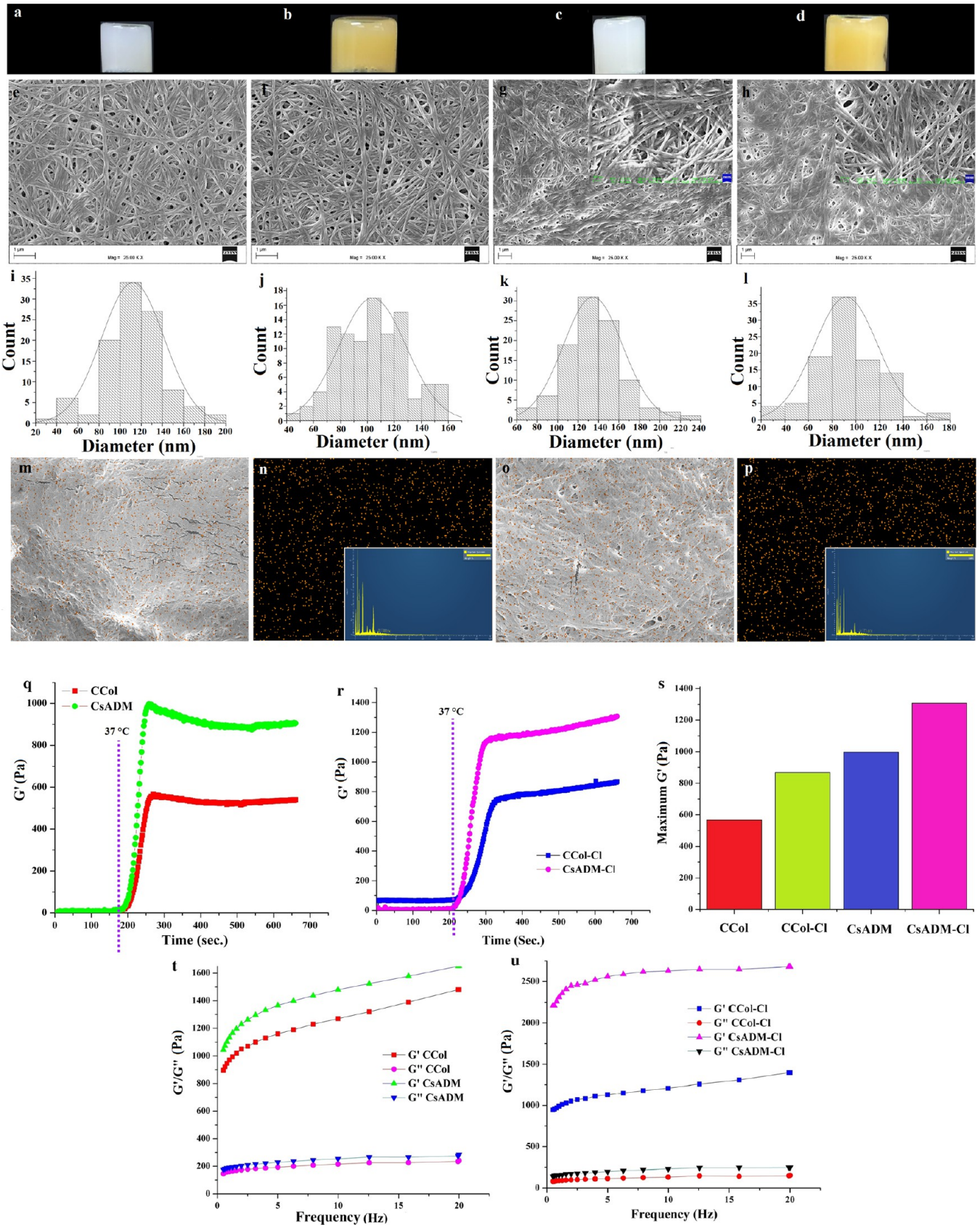

Figure 2. Crosslinking enhances viscoelastic properties, while retaining nanofibrillar hydrogel architecture. Optical images, surface topology, and fiber network analysis of CCol (a,e,i), CCol-Cl (b,f,j), CsADM (c,g,k), and CsADM-Cl (d,h,l); inset (g & i) shows magnified images. EDX mapping of iodine on the fibrillar network of CCol-Cl (m,n) and CsADM-Cl (o,p). Gelation kinetics of hydrogel (q) without a crosslinker (CCol and CsADM) and (r) with a crosslinker (CCol-Cl and CsADM-Cl); (s) maximum elastic modulus (G'); frequency sweep analysis post gelation for (t) uncrosslinked (CCol and CsADM); and (u) crosslinked (CCol-Cl and CsADM-Cl) samples.

https://dx.doi.org/10.1021/acs.biomac.0c01400
Biomacromolecules 2021, 22, 514−533

determined using NanoDrop (NanoDrop 2000/2000c, Thermo, USA) (high quality RNA has OD 260/280 nm ratio between 1.8 and 2.0), and equivalent RNA of each group was reverse transcribed to cDNA using the cDNA synthesis kit (Thermo Scientific, USA), following the manufacturer's protocol. The primer sequences used for the study are given in the Supporting Information.

2.16. Statistics. GraphPad Prism software (version 5.02, La Jolla, CA, USA) was used to execute statistical evaluations of data obtained from different groups. All experiments were repeated thrice unless mentioned, and the data signifies mean ± SD. The level of significance was determined as $P < 0.05$.

3. RESULTS

Hybrid hydrogels (CCol, CCol-Cl, CsADM, and CsADM-Cl) were fabricated successfully at physiological pH and temperature using CTS, DHF-I, and ADM/Col. The possible mechanism of hydrogel formation with ADM/Col and crosslinking reaction by CTS and DHF-I is shown in Scheme 1. Interestingly, both CCol-Cl and CsADM-Cl were observed to be injectable using a syringe with 18 G needle. Uncrosslinked hydrogels took 15 ± 2 min for gelation, while crosslinked hydrogels gelled within 5 ± 1 min at 37 °C.

3.1. Extraction of sADM and Col. The ADM was successfully prepared from rat dermis by a combinatorial treatment of trypsin and Triton X-100. After decellularization, the NS turned milky white from pinkish red, which represents the removal of cells. The efficiency of the decellularization process was confirmed using H&E, Col I, AB, and DAPI staining. The ADM, in contrast to the NS, showed the absence of any cell nucleus as observed by H&E and DAPI staining, whereas major protein Col and GAGs had similar intensity in both NS and ADM sections as shown by Col I and AB staining, respectively (Figure 1a). SDS-PAGE (Figure 1b) shows the existence of a mixture of proteins/peptides in the ADM as evident from the presence of different molecular weights bands, especially bands at a lower molecular weight. Such an observation signifies the preservation of bioactive molecules in the ADM post decellularization. The absence of the DNA fragment in the ADM was demonstrated by the GelDoc image (Figure 1c), which corroborates with the findings of H&E and DAPI staining. The NS and ADM were processed to isolate and to quantify DNA. In comparison to the NS (1121 ± 210 ng/mg dry weight), the ADM showed significantly reduced ($p < 0.001$) DNA content (30.14 ± 12.34 ng/mg dry weight), as observed in Figure 1d. Further, Col content of the NS and ADM did not show any significant difference; the Col content in the ADM was 60.12 ± 5.31% of dried tissue, whereas in the NS, it was 52.31 ± 4.61% of dried tissue (Figure 1d). Also, sGAG content was not observed to vary significantly in the ADM (0.44 ± 0.06% dry weight) when compared to NS (0.512 ± 0.07%) (Figure 1d). The presence of essential growth factors (BMP-2, VEGF, and TGF-β) was revealed through ELISA assay in both the NS and ADM (Figure S1a).

The isolated rat tail Col was characterized using SDS-PAGE. Rat tail Col demonstrated a classic band pattern for type I Col, that is, a doublet at molecular weights ∼215 and ∼235 kDa; also, an additional doublet at ∼115 and ∼130 kDa was observed in SDS-PAGE (Figure S1b).

3.2. DHF-I Synthesis. Iodine reacts with the double bond of DHF *via* electrophilic addition reaction and formed DHF-I which was confirmed through ^{1}H NMR analysis of pristine DHF and DHF-I. In the ^{1}H NMR (Figure S2a) spectrum of DHF, the chemical shifts between δ = 3.49−3.52 ppm signify methoxy proton (H1) of cis and trans isomers. The chemical shifts between δ = 6.27−6.29 ppm are because of H2 protons. The chemical shifts at δ = 5.78 and 6.07 ppm are due to the presence of unsaturated protons (H3). The disappearance of the chemical shift at δ = 5.78 ppm and the appearance of a new chemical shift between δ = 3.78−3.82 ppm in the NMR spectrum of an iodinated product reveal the successful formation of DHF-I from DHF through iodination reaction.

3.3. Macroscopic Appearance of Hydrogel. Uncrosslinked hydrogels (CCol/CsADM) were softer with round edges in comparison to crosslinked hydrogels (CCol-Cl/CsADM-Cl), which were observed to be rigid structures with defined edges and easy to handle with the help of tweezers (Figure 2a−d). SEM analysis of the hydrogel microstructure revealed a nano-fibrillar morphology in both groups, that is, CCol (Figure 2e) and CsADM (Figure 2g). Further, crosslinking of hydrogels did not affect adversely the intrinsic property of the self-assembly into a nano-fibrillar structure, and a similar structure was observed in CCol-Cl (Figure 2f) and CsADM-Cl (Figure 2h). After crosslinking, the fiber diameter was reduced marginally; the fiber diameters of CCol, CCol-Cl, CsADM and CsADM-Cl hydrogel were ∼110, ∼105, ∼135, and ∼95 nm, respectively (Figure 2i−l). The presence of iodine in the crosslinked matrix was confirmed by EDAX scanning; both crosslinked hydrogel variants CCol-Cl (Figure 2m,n) and CsADM-Cl (Figure 2o,p) showed uniform iodine distribution.

3.4. Hydrogel ICC. For evaluating the presence of characteristic ECM biomolecules such as Col I and fibronectin, ICC was performed against specific antibody (Figure S3). The distribution of ECM active biomolecules was similar in NS and ADM. Also, cytokines and growth factors that are vital for dermal neovascularization and regeneration, like TGF-β, VEGFA, MCP-1, and IL-8, were also evaluated in the NS, ADM, and CsADM and CsADM-Cl hydrogels. The ICC results revealed the fact that although intensity of the ICC stains diminished, yet part of each growth factor was preserved in the crosslinked hydrogel (Figure S3). Altogether, the native nanofibrillar structure and bioactive components were well preserved after crosslinking with CTS and DHF.

3.5. Rheological Characterization of Hydrogel. The rheological properties of hybrid hydrogel were studied using a parallel plate rheometer (Figure 2q−u). The average viscosity at 25 °C of pregel solution was 1.5 and 1.9 Pa s for CCol and CsADM, respectively. Storage modulus (G') and loss modulus (G'') increase with an increase in temperature from 15 to 37 °C (Figure 2q,r). The G' value was higher than G'' for both the variants by a factor of ∼5, which denotes the solid-like behavior of pregel solutions after gelation. The steady-state G' after complete gelation varied non-linearly with temperature/time, and when compared to a uncrosslinked variant, the crosslinked variant showed higher G' (Figure 2s). After gelation, frequency response was studied, and the value of G' was independent of frequency (Figure 2t,u), indicating the frequency-independent gelation behavior. At all frequencies, crosslinked hydrogel showed higher G' when compared to the uncrosslinked variant, representing superior stability and strength.

3.6. FTIR. FTIR spectra of CCol, CCol-Cl, CsADM, and CsADM-Cl are shown in Figure S2b. The CCol hydrogel (Figure S2b(A)) showed peaks at 3357, 2982, 1640, 1578, and 1414 cm^{-1} which are responsible for frequencies of N−H bond stretching (amide A), C−H stretching, amide-I stretching,

https://dx.doi.org/10.1021/acs.biomac.0c01400
Biomacromolecules 2021, 22, 514−533

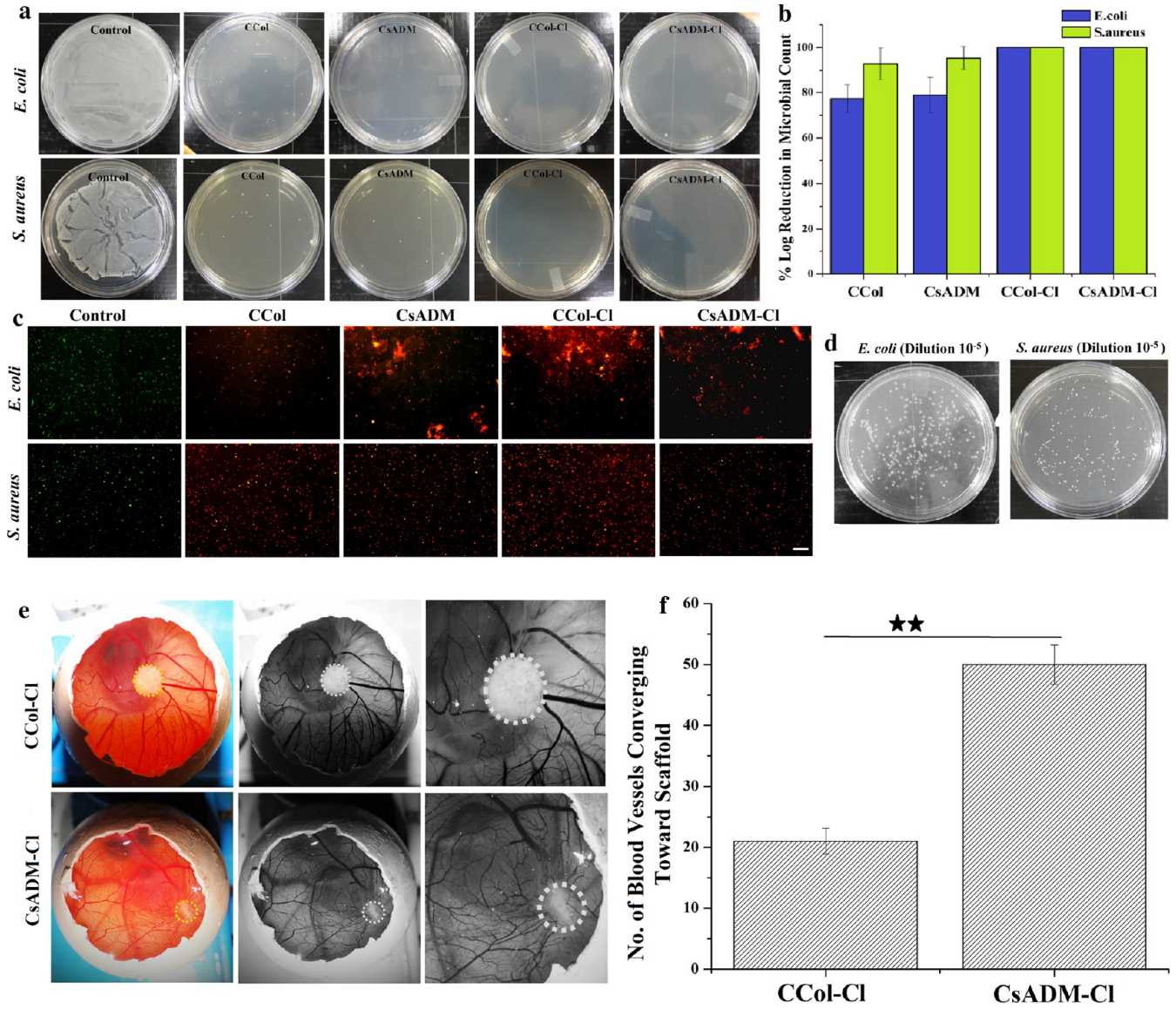

Figure 3. Antimicrobial and angiogenic potential, both are important in wound healing applications. Microbes (*E. coli* and *S. aureus*) colony grown on an agar plate after contact with control and hydrogel (a); log reduction in microbial count (b); Live/Dead staining post 2 h of incubation with hydrogel (c); and culture plates of control-treated *E. coli* and *S. aureus* (10−5 dilution) (d). CAM assay macroscopic view (e) and quantification of vessels (f) growing toward scaffolds. *Y*-error bars represent SD, ** signifies $p < 0.01$, and scale bar represent 50 μm.

amide-II stretching, and amide III stretching, respectively. The crosslinked hydrogel (Figure S2b(B)) CCol−Cl exhibited peaks for amide A, C−H stretching, amide I, amide II and amide III at 3340, 2972, 1634, 1556, and 1405 cm^{-1}, respectively, while the CsADM hydrogel (Figure S2b(C)) demonstrated peaks of N−H stretching, C−H stretching, amide I, amide II, and amide III at 3366, 2982, 1633, 1567, and 1414 cm^{-1}, respectively. The crosslinked hydrogel (Figure S2b(D)) CsADM-Cl exhibited peaks for amide A, C−H stretching, amide I, amide II, and amide III stretching frequencies at 3325, 2982, 1634, 1556, and 1409 cm^{-1}, respectively. Further, the increase of peak intensity at 1634 cm^{-1} for both crosslinked hydrogels (Figure S2b(B,D)) implies the formation of the Schiff base by chemical crosslinking between CTS, collagen/sADM, and the iodinated DHF *via* imine (C═N) bond.[38]

The triple helix integrity of Col fibers in both isolated Col and ADM is a critical factor attributing to good combination of mechanical and biological properties.[44] This further will dictate the hydrogel behavior *in vivo*. The ratio of O.D. 1235 cm^{-1} and O.D. 1450 cm^{-1} can assess Col's triple helix integrity. Also, values around 0.5 have been reported for denatured, while those around 1 indicate native triple helix structures.[45,46] In case of the blend samples (CCol and CsADM), the values obtained were 1.01 and 1.00, respectively. Similarly, the values obtained were 1.03 and 1.04 for crosslinked samples CCol-Cl and CsADM-Cl, respectively. Such observations indicate that the crosslinking did not destabilize the triple helix structure. Absence of band at 1706 cm^{-1} (corresponding to free acetic acid)[45] in any of the groups evidences complete neutralization of the hydrogels, which is essential for imparting the bioactive biocompatible surface *in situ* for neighboring cell infiltration and proliferation.

3.7. Iodine Release Kinetics. Figure S4 demonstrates the iodine release curves of the CsADM-Cl hybrid hydrogel in PBS and buffered enzymatic solution at a different predetermined

https://dx.doi.org/10.1021/acs.biomac.0c01400
Biomacromolecules 2021, 22, 514−533

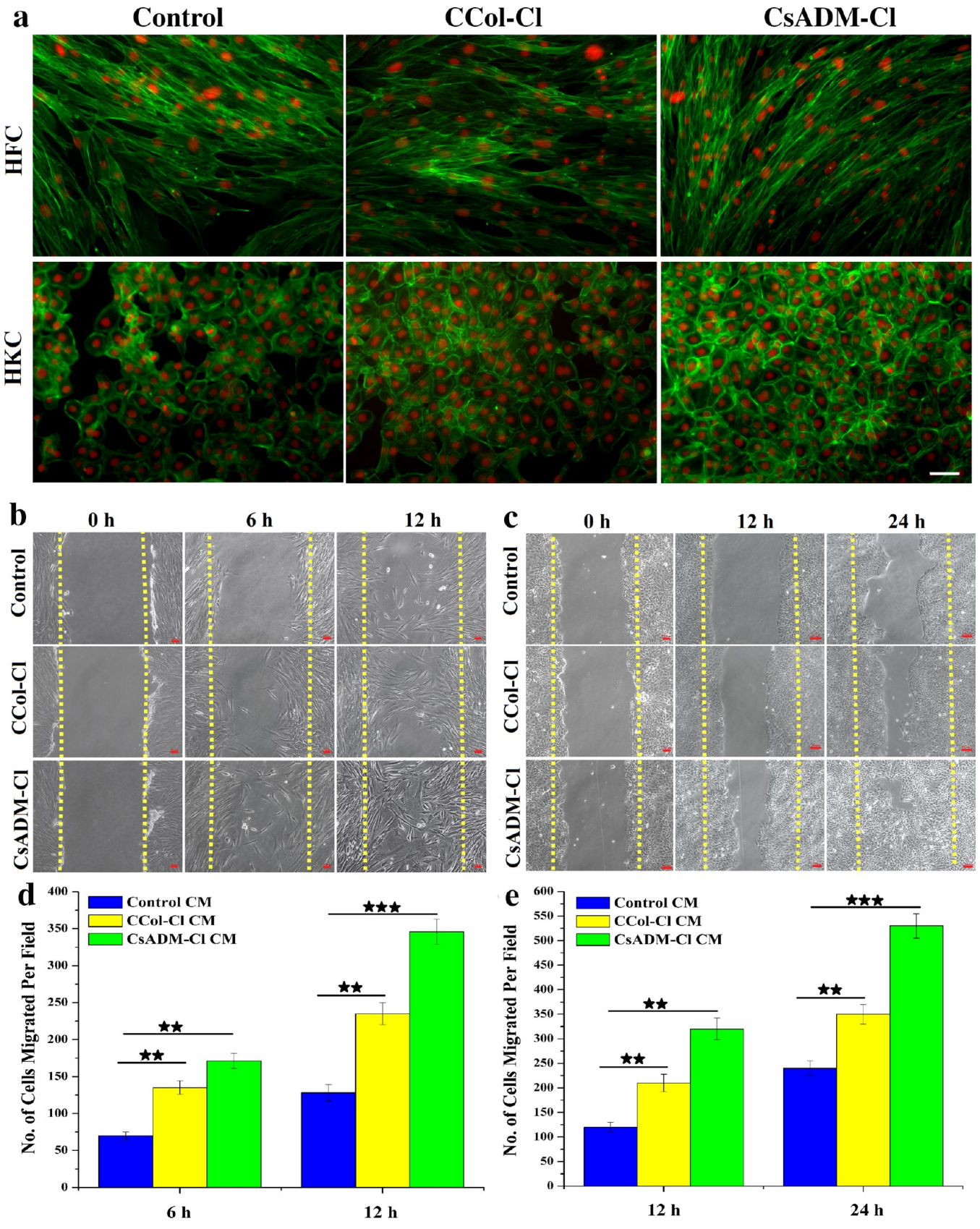

Figure 4. Crosslinked hybrid hydrogels exhibit better cytocompatibility and cell migration behavior of skin tissue cells. Rhodamine phalloidin−DAPI images of HFCs and HKCs cultivated in CCol-Cl and CsADM-Cl-conditioned medium at different time durations; cell migration quantification of (d) HFCs and (e) HKCs. (Scale bar represents 50 μm, red represents nucleus staining DAPI; and green depicts cytoskeleton expression). *Y*-error bars represent SD, ** represent $p < 0.01$, and*** signifies $p < 0.001$.

https://dx.doi.org/10.1021/acs.biomac.0c01400
Biomacromolecules 2021, 22, 514−533

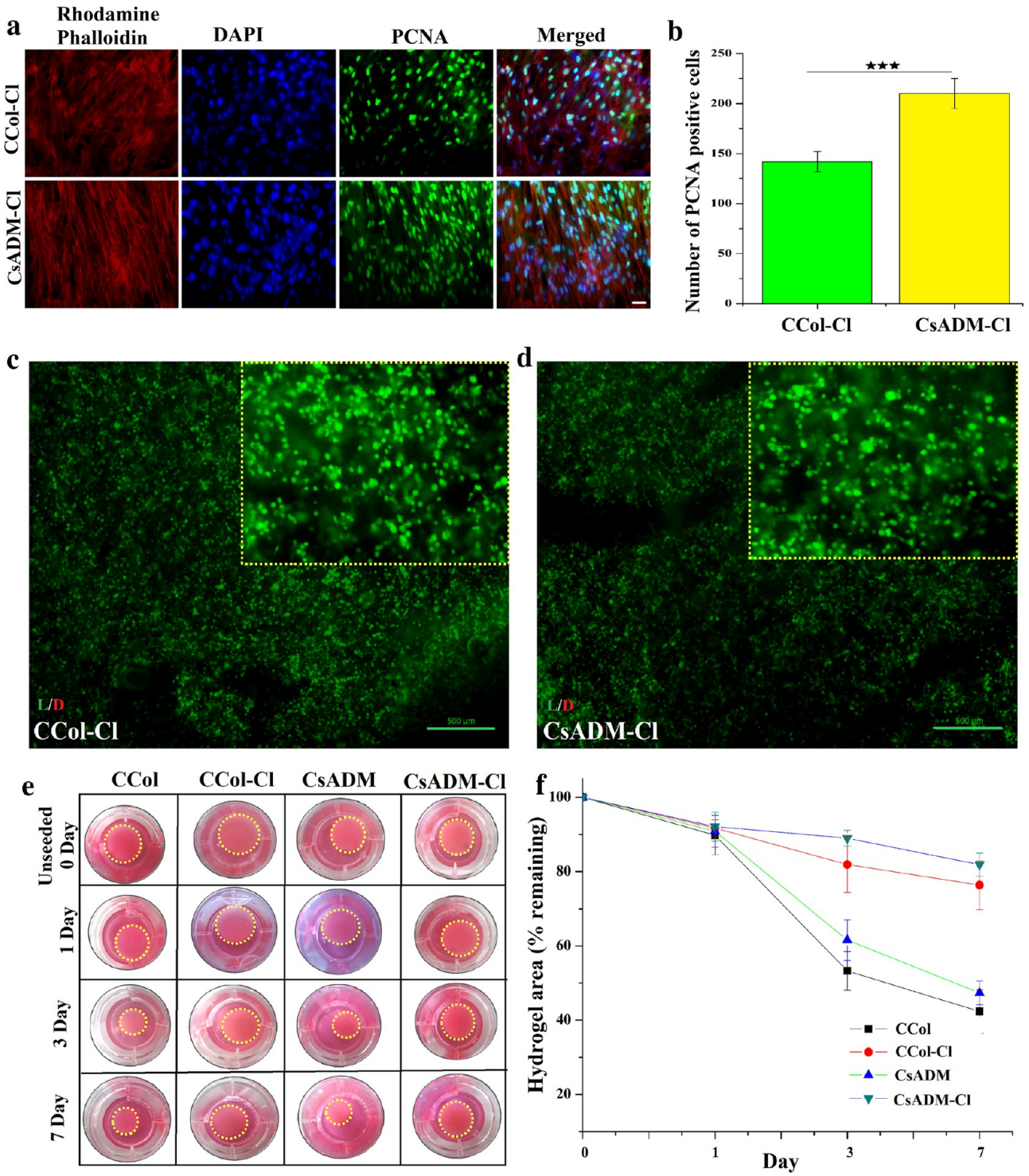

Figure 5. Quantitative and qualitative cell infiltration and proliferation of HFC-encapsulated hybrid hydrogels. PCNA staining images (a) and quantification of PCNA positive cells (b) of HFCs cultivated in CCol-Cl and CsADM-Cl. Live/Dead staining images of CCol-Cl (c) and CsADM-Cl (d) encapsulated with HFCs post 72 h of incubation; images of contraction of HFCs seeded hybrid hydrogels at different time periods (e) and quantification of area remaining (f). Scale bar represents 50 μm; *Y*-error bars represent SD; and *** signify $p < 0.001$.

period. The iodine release rate from hydrogel was slower in PBS when compared to the enzymatic solution. There was an initial rapid release (in PBS: 1919.84 ± 105.9 ppm; in enzyme: 3771.51 ± 163.4 ppm) at 6 h of incubation. Further, the CsADM-Cl hydrogel showed a prolonged release behavior of iodine (in PBS: 2190.67 ± 106.5 ppm; in enzyme: 3959.35 ± 191.23 ppm) till 24 h, after which it attained the plateau phase.

3.8. Antioxidant Assay. Antioxidant molecules have been reported to exert a positive effect on wound healing progression and pace by regulating burden of excess reactive oxygen species (ROS) in the wound site.[47] Thus, iodine introduction in the hydrogel matrix plays another vital role since iodine has an antioxidant activity.[48] Antioxidant potential was evaluated by measuring the efficiency of hydrogels to

https://dx.doi.org/10.1021/acs.biomac.0c01400
Biomacromolecules 2021, 22, 514−533

scavenge DPPH. All hydrogels showed differential reduction in the DPPH peak, which was attributed to hydrogen atom donation or electron transfer from the parent molecule to DPPH free radical. The DPPH scavenging efficiency of CCol, CsADM, CCol-Cl, and CsADM-Cl was 19.54 ± 0.9, 24.14 ± 2.12, 58.60 ± 5.21, and 63.20 ± 6.21%, respectively (Figure S2c). These results demonstrated that crosslinked variants had significantly ($p < 0.001$) superior antioxidant potential when compared to uncrosslinked variants. Also, hybrid hydrogels can prevent cell damage and enhance viability by reducing excess ROS *in vitro*.

3.9. Hemocompatibility. Blood compatibility of the skin substitute is important because it would stimulate the blood defense systems (*i.e.*, coagulation or fibrinolysis) which can further worsen the situation.[49] Hemocompatibility is especially essential for FT/critical burn wounds with significant loss of skin components (either epidermis or epidermis dermis both) and hence bringing the skin substitute in direct contact to different body fluids. The percentage hemolysis is a direct indicator of the extent of erythrocyte damage when exposed to sample of interest. CCol-Cl, CsADM-Cl, positive control (Triton X-100), and negative control (saline) on direct contact with RBCs showed an absorbance of 0.047 ± 0.02, 0.048 ± 0.01, 0.6835 ± 0.02 and 0.038 ± 0.01, respectively. The percentage hemolysis due to CCol-Cl/CsADM-Cl was 1.39 ± 0.12 and 1.55 ± 0.13%. Generally, hemolysis <5% is acceptable for a suitable biomaterial to be used *in vivo*. Higher percentage of hemolysis reveals biomaterial's poor hemocompatibility. All materials used clinically in current practice, including PVC, meet these guidelines.[50] The data suggested that CCol-Cl and CsADM-Cl can exhibit clinically desired hemocompatibility.

3.10. Antibacterial Assay. Burn wounds are prone to bacterial infection.[51] Therefore, dressings with the inherent antibacterial property will be beneficial to remove the bacterial load and inflammatory response from the wounds. Iodine is reported to exhibit a significant antibacterial property even at 1 ppm.[51,52] For demonstrating antibacterial activity, hydrogels were challenged with two pathogens (*E. coli* and *S. aureus*) at a concentration of about 10^6 cfu, and the cell-count reductions after 2 h treatment were recorded post incubation for 12 h in agar gel. Figure 3a−d shows the antibacterial activity of the hydrogel. CCol and CsADM exhibited good activity against Gram positive and Gram-negative bacteria. CCol and CsADM showed a log reduction of 7.72 ± 4.2 and 7.89 ± 3.5 against *E. coli*, respectively, whereas 8.39 ± 5.2 and 8.55 ± 3.4 against *S. aureus*, respectively (Figure 3b). The control group displayed development of lawn post direct plating (Figure 3a). For calculating log reduction, cfu from 10^5 dilution (Figure 3d) in control was utilized. On other hand, all DHF-I crosslinked hydrogel, that is, CCol-Cl and CsADM-Cl demonstrated outstanding antibacterial property (Figure 3a). No survival colony was observed after incubation for 12 h in agar gel. Further, Live/Dead assay also revealed the presence of red stained cells denoting non-viable bacterial cells on the hydrogel surface (Figure 3c).

3.11. CAM Assay. Capillary formation on CAM was observed to investigate the angiogenesis potential of CCol-Cl and CsADM-Cl hydrogels (Figure 3e,f). After incubation with the CCol-Cl/CsADM-Cl disc for 3 days, the embryo was alive, indicating the non-toxic nature of hydrogel. Further, the blood vessels were also found to be branched therein. Interestingly, after 72 h of incubation, there were significantly ($p < 0.001$) higher number of blood vessels approaching toward the CsADM-Cl hydrogel (50 ± 3) when compared to CCol-Cl (21 ± 2) hydrogel on treated CAM. Moreover, CsADM-Cl-treated CAM led to a higher number of branch points when compared to CCol-Cl-treated CAM.

3.12. *In Vitro* Assays. *3.12.1. Indirect Assay.* To evaluate the toxicity of the eluted remnant material hydrogels conditioning media, treated cells were stained using rhodamine phalloidin/DAPI. HFCs and HKCs showed a similar morphology in a conditioned medium like control after 72 h of incubation (Figure 4a). HFCs treated with the CsADM-Cl conditioning media displayed a well-spread cytoskeleton and extended F-actin filaments, revealing a higher cell-to-cell contact.

In vitro, wound healing or scratch assay was also performed to evaluate the effect of conditioning media on the proliferation potential of HFCs. Interestingly, none of the group showed an adverse effect on the proliferation rate of HFCs when treated for 24 h. Wounds/scratches treated with CCol-Cl/CsADM-Cl conditioning media showed a significantly ($p < 0.01$) higher rate of migration of HFC in the denuded path after 6 h of treatment (Figure 4b,d). After 12 h of treatment, the CsADM-Cl-treated group showed complete wound coverage (100%) in comparison to control (68.675 ± 5.61%) and CCol-Cl (80.52 ± 6.21%). Similarly, in the case of HKCs, they were observed to follow an increasing trend of migration with time. A significantly higher migration rate ($p < 0.001$) of HKCs was supported by the conditioning media of CCol-Cl/CsADM-Cl, as observed in Figure 4c,e. After 24 h of treatment, the CsADM-Cl conditioning media-treated group showed a wound closure of 93.12 ± 2.11% in comparison to the control of 33.56 ± 1.24% and the CCol-Cl conditioning media-treated group of 64.00 ± 3.44% ($p < 0.001$).

3.12.2. Direct Assay. HFCs were directly plated on hydrogel-coated coverslips and subjected to MTT assay to assess the metabolic activity, proliferation assay (PCNA) to identify actively proliferating cells, and apoptosis staining to identify apoptotic cells. Both HFCs and HKCs showed an increasing growth trend of metabolically active cells with time, revealing the non-toxic behavior of CCol-Cl/CsADM-Cl. The proliferation rate of cells was significantly ($p > 0.05$) higher in the CsADM-Cl treated group when compared to CCol-Cl (Figure S5a,b). After 5 days of cultivation, there was a significantly ($p > 0.001$) higher number of PCNA positive cells (Figure 5a,b) in CsADM-Cl (210 ± 15) when compared to CCol-Cl (142 ± 8). Also, cells cultivated on CCol-Cl showed significantly ($p > 0.001$) higher number of PCNA positive cells when compared to that on control. Further, there were no apoptotic cells in any of the group (Figure S5c), demonstrating the excellent cellular compatibility of the hydrogel.

3.12.3. HFC Encapsulation in Hydrogel. Figures 5c,d and S6 represent the cells encapsulated into hydrogels. It is noticeably demonstrated that the majority of cells were alive, depicting green fluorescence post 72 h of incubation in hydrogels, suggesting that the dual crosslinked nanofibrillar microenvironment were non-toxic to the HFCs.

3.12.4. ECM Hydrogel Contraction. Hydrogels showed an increased contraction, when incubated from 12 h to 7 days in culture. Also the contraction rate relied on the crosslinking status of the hydrogel (Figure 5e,f). The unseeded hydrogel area remained the same regardless of being crosslinked/uncrosslinked/left for different time points (data not shown). Hydrogel contraction (Figure 5f) in CsADM-Cl (81.88 ± 3.1%) and CCol-Cl (76.35 ± 6.5%) hydrogel groups was

https://dx.doi.org/10.1021/acs.biomac.0c01400
Biomacromolecules 2021, 22, 514−533

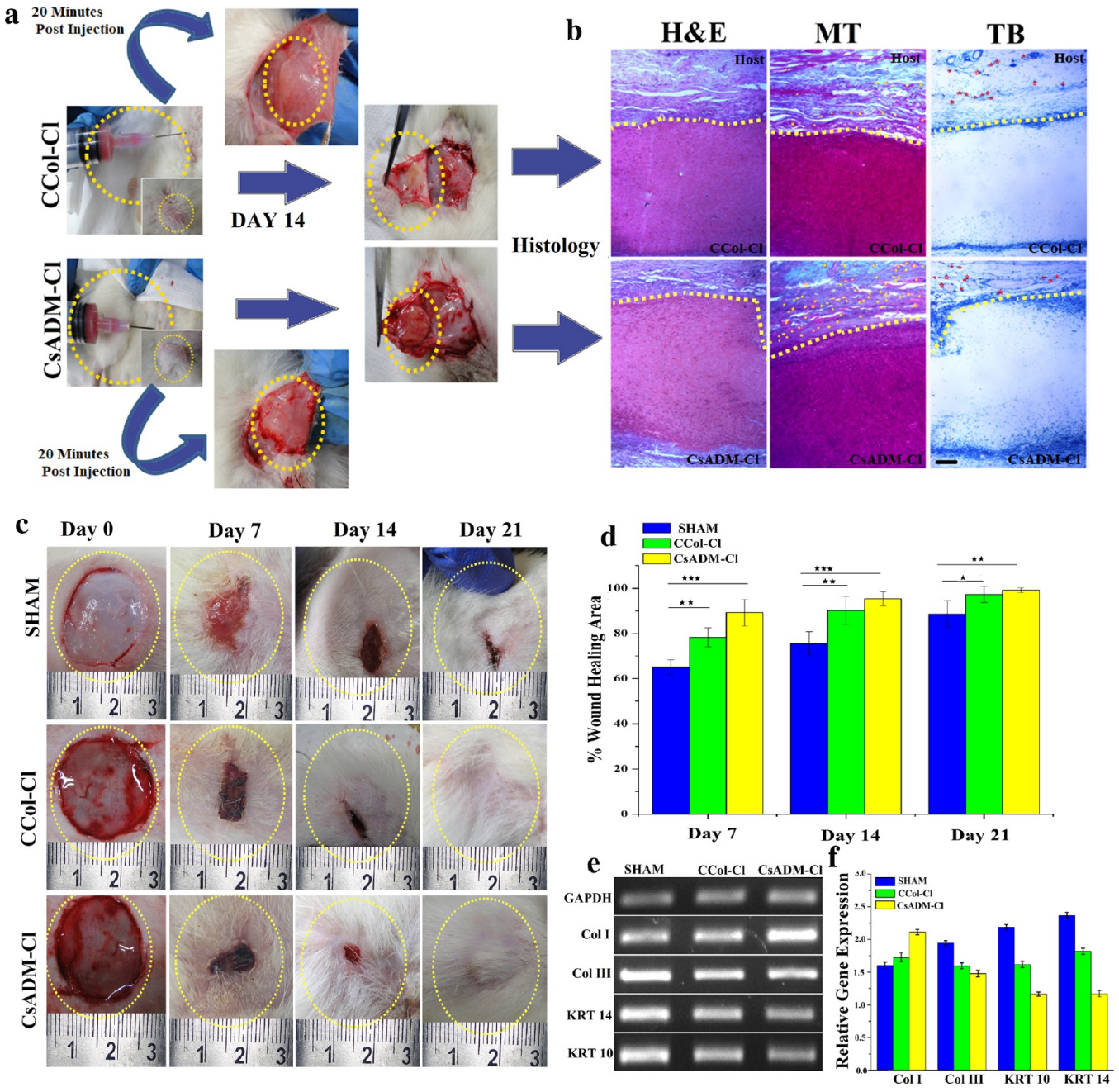

Figure 6. Pre-clinical study in a rat model. Biocompatibility of subcutaneously injected hybrid hydrogels (CCol-Cl and CsADM-Cl) was evaluated in dorsal skin in a rat model (a) and histological study post 10 days of injection (b). Healing progression of full-thickness cutaneous wounds treated with SHAM, CCol-Cl, and CsADM-Cl; optical images of wounds (c) and wound closure rate (d) on days 0, 7, 14, and 21; (e and f) RT-PCR analysis at 21 day post wounding. Yellow star represents the blood vessel in MT staining (b), red star in TB staining represents TB-positive stained cells (b), yellow dotted line represent adjoining area between the host and implant (b), and yellow circle area of interest (b). Scale bar represents 50 μm; *Y*-error bars represent SD, yellow dotted circle represent wound area (c),* signifies $p < 0.05$, ** signifies $p < 0.01$, and *** signifies $p < 0.001$.

significantly lesser when compared to CCol (42.35 ± 5.89%) and CsADM (47.35 ± 3.2%) groups. Crosslinking imparted stability to hydrogel networks. Hence, crosslinked hydrogels were observed to contract lesser when compared to uncrosslinked hydrogels.

3.13. Host Response to the Hydrogel. To evaluate the host response to hydrogel, CCol-Cl/CsADM-Cl was injected subcutaneously in the rat. The treated groups were observed to be healthy, and there were no mortality during the study. The rat weight did not vary abruptly during the study period (data not shown). After 2 weeks of injection, CCol-Cl/CsADM-Cl was retrieved along with the surrounding tissue and was subjected to histological staining for studying the interaction between the hydrogel and the host tissue, as shown in Figure 6a,b. H&E staining demonstrated host tissue integration with CCol-Cl/CsADM-Cl and also host cell infiltration in hydrogel was evident. Interestingly, as displayed in Figure 6b, CsADM-Cl showed more infiltration and proliferation of cells, as compared to CCol-Cl.

https://dx.doi.org/10.1021/acs.biomac.0c01400
Biomacromolecules 2021, 22, 514−533

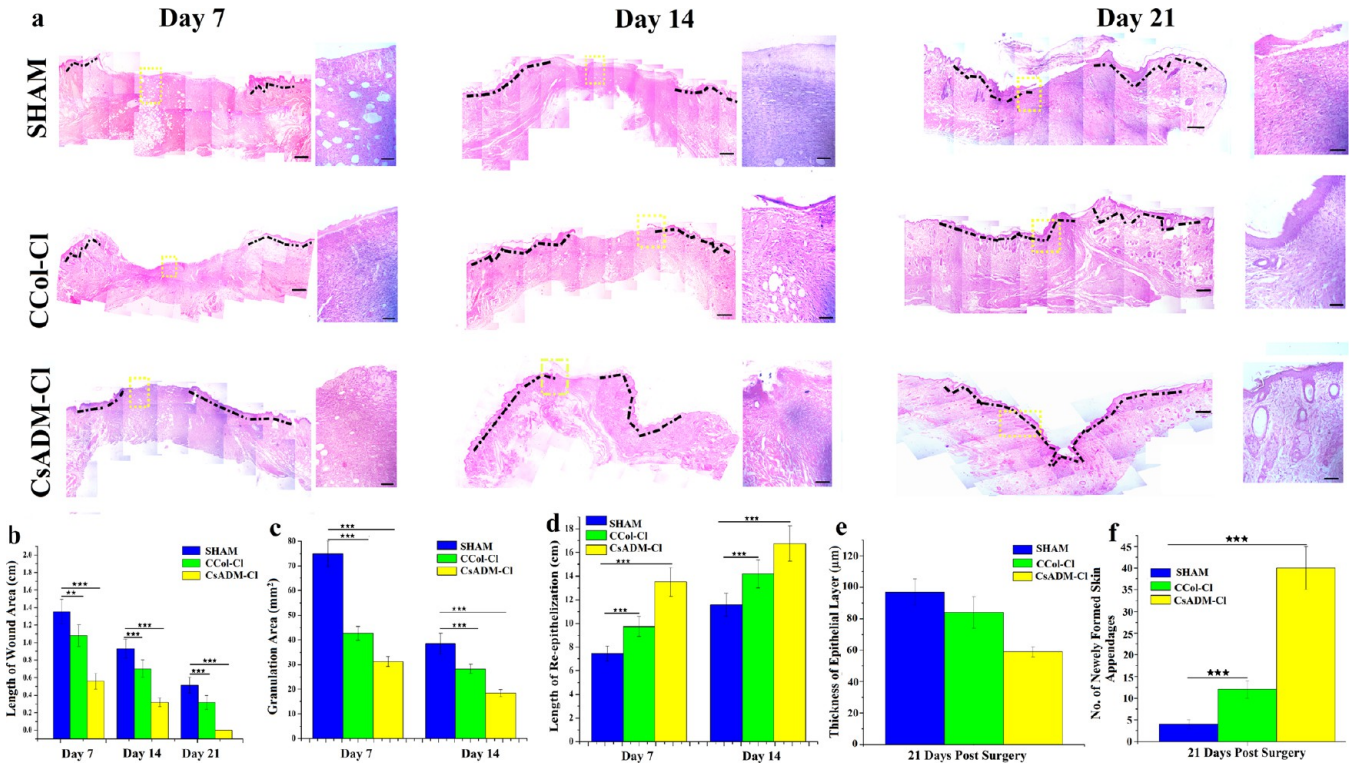

Figure 7. Histomorphometric analysis provides quantitative wound healing efficacy of injectable hybrid hydrogels. Histological micrographs of wound sections implanted with CCol-Cl and CsADM-Cl at days 7, 14, and 21 after dermal excision by H&E staining (a), quantification of length of wound area (b), granulation area (c), length of reepithelization (d), thickness of epithelial layer (e), and no. of newly formed skin appendages at predetermined period (f). Scale bar represents 50 μm; black dotted line represent healed area; ** signifies $p < 0.01$, and *** signifies $p < 0.001$.

MT staining of the retrieved hydrogels showed absence of capsular layer/fibrosis and the presence of blood vessels in the interface area. Further, the interfacial layer was also characterized by the presence of dense collagen fiber deposition, demonstrating stimulated cell infiltration in CCol-Cl/CsADM-Cl. To assess inflammatory response to hydrogel, TB staining was performed. TB staining revealed very few mast cells near the implanted zone, and also, there were no mast cell infiltration inside CCol-Cl/CsADM-Cl. This minimal inflammatory response after CCol-Cl/CsADM-Cl injection is similar to the normal wound healing cascade. These findings establish the biocompatible nature of CCol-Cl and CsADM-Cl and also demonstrate that neither of hydrogels triggered an adverse immune response *in vivo*.

The plausible toxicity of CCol-Cl/CsADM-Cl to vital organs was also determined by retrieving major organs after two-week post-injection. Major organs (liver, kidney, lung, and heart) retrieved were analyzed *via* histological staining, and there were no significant necrosis or pathological changes in the anatomy of the organs of the CCol-Cl/CsADM-Cl-treated group in comparison to the untreated group (Figure S7). Cardiac muscles in the heart had the similar anatomy for all groups, and also there was the absence of any sign of fibrosis or inflammation. Hepatocyte distribution in the liver of treatment groups showed the normal anatomy. Also, lungs had no signs of fibrosis in treatment groups. Moreover, in kidney sections, glomerulus structure was distinctly visible for all groups. These results signify that CCol-Cl and CsADM-Cl did not exert any toxic effect on major organs in the rat model.

3.14. Hydrogel Treatment of Dorsal Burn Injury Model. Burn model was prepared as demonstrated in Figure S8; FT wounds created post burn injury were treated with crosslinked hybrid hydrogels CCol-Cl/CsADM-Cl, whereas Tegaderm covered wounds were marked as the SHAM group, which served as a control for the study. Tegaderm was also placed on top of hydrogels to secure their position on the wound bed. Animals were sacrificed after a predetermined period, that is, 7, 14, and 21 days post-treatment for histological analysis. Optical images revealing the morphological changes in wound closure for various groups are provided in Figure 6c,d. Wound treated with CsADM-Cl showed significantly enhanced wound closure (~89.23% healing) 7 days post-surgery when compared to groups treated with CCol-Cl (~78.21% healing)/SHAM (~65.11% healing) (Figure 6d).

By day 14, ~90.21 and ~95.40% of the wounded area were re-epithelialized in wounds treated with CCol-Cl and CsADM-Cl, respectively. This was significantly higher than the SHAM group (~75.52%). 21 days post-surgery CsADM-Cl-treated groups showed complete wound closure, that is, ~99.12%, while CCol-Cl/SHAM groups were still in the healing phase. However, CCol-Cl (~97.254%)-treated groups showed significantly higher % healing when compared to the SHAM group (~88.62) on day 21 (Figure 6d). All these findings suggest that the wound treated with CsADM-Cl showed enhanced wound closure and hence better-wound healing as compared to CCol-Cl/SHAM groups.

3.15. Histomorphometric Analysis. Wound healing is a multifaceted repair process involving recruitment of cells to the wound area by releasing chemoattractants, followed by cell proliferation and differentiation. These pathobiological processes lead to the formation of new tissue and hence wound closure. To further analyze the healing progression in different groups, H&E staining was performed to detail the morpho-

https://dx.doi.org/10.1021/acs.biomac.0c01400
Biomacromolecules 2021, 22, 514−533

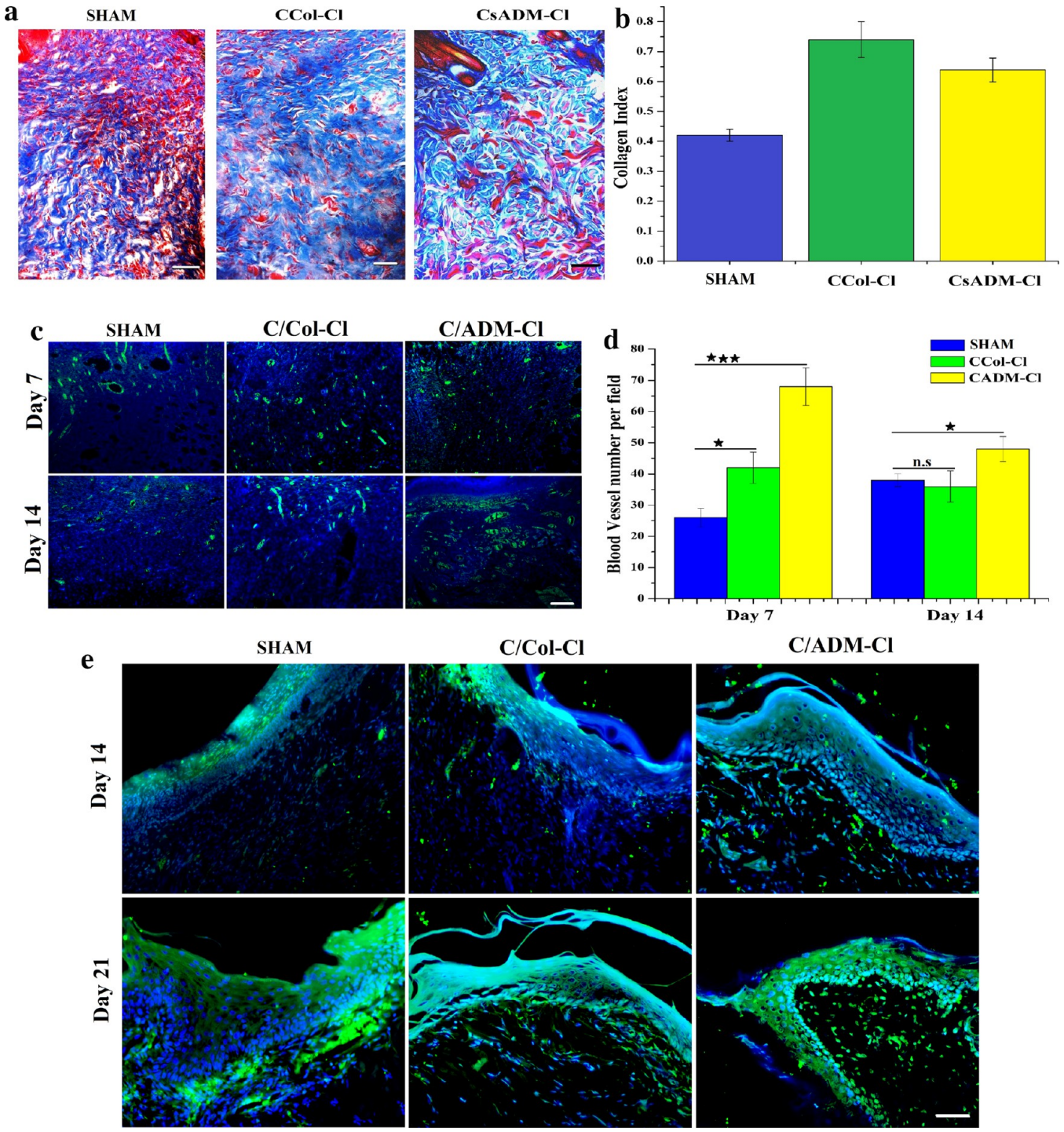

Figure 8. Collagen staining and immunohistochemical analysis demonstrated the potential of the hybrid hydrogels to heal chronic wounds in a rat model. MT staining (a) and quantification of collagen index (b) 21 days post treatment with CCol-Cl and CsADM-Cl. Representative IHC images of anti CD-31 (c) and anti CK-10-(e) stained histological sections on determined periods. Quantification of blood vessels on day 7 and day 14 of wounds treated with SHAM, CCol-Cl, and CsADM-Cl (d). Scale bar represents 50 μm; red represents nucleus staining DAPI, and green depicts antibody expression; *Y* error bar represent SD; ** signifies $p < 0.01$, and *** signifies $p < 0.001$.

logical changes in different layers of skin (Figure 7). At day 7 post surgery, the length of the wound reduced significantly in wounds treated with CsADM-Cl (0.56 ± 0.09 cm) and CCol-Cl (1.08 ± 0.12 cm) when compared to the SHAM group (1.36 ± 0.14 cm). In addition, CsADM-Cl-treated wounds demonstrated significantly enhanced re-epithelialization (13.49 ± 1.2 cm) accompanied with lower area of granulation (31.26 ± 2.05 mm^2). This was characterized with a thicker and well-organized granulation tissue when compared to the CCol-Cl (re-epithelialization 9.74 ± 0.85 cm and Granulation area 42.69 ± 2.87 mm^2)/SHAM treated group (re-epithelialization 7.46 ± 0.65 cm and Granulation area 74.97 ± 5.21 mm^2) (Figure 7b–d). Granulation tissue formation is an essential aspect of wound repair and regeneration. The granular tissue is composed of synthesized ECM, fibroblasts, and bioactive molecules, dictating the different phases of healing.[52−56] By

https://dx.doi.org/10.1021/acs.biomac.0c01400
Biomacromolecules 2021, 22, 514−533

day 14, the length of wounds (control: 0.9307 ± 0.11 cm, CCol-Cl: 0.7026 ± 0.1 cm, CsADM-Cl: 0.3187 ± 0.05 cm) and granulation area (control: 38.447 ± 4.21 mm^2, CCol-Cl: 28.293 ± 1.92 mm^2, CsADM-Cl: 18.368 mm^2) further decreased, whereas the length of reepithelization (control: 11.578 ± 0.98 cm, CCol-Cl: 14.189 ± 1.18 cm, CsADM-Cl: 16.749 ± 1.48 cm) increased, indicating healing progression in all the groups (Figure 7b−d).

At 21 days post-surgery, no wound was observed in groups treated with CsADM-Cl, whereas CCol-Cl and control-treated group showed a wound length of 0.514 ± 0.09 and 0.319 ± 0.08 cm, respectively (Figure 7b). The CsADM-Cl-treated group exhibited complete re-epithelization with a defined epidermal−dermal junction, when compared to the CCol-Cl/control group. The epidermal−dermal junction forms a surging interdigitating interface (inset of Figure 7), which increases the surface area and hence strengthening the contact between the dermis and epidermis. Also, the CsADM-Cl-treated group exhibited a significantly higher number of newly formed appendages (40 ± 5) when compared to the CCol-Cl (12 ± 2)/control (4 ± 2)-treated group (Figure 7f). The newly formed appendages in the wound area signify a better quality of wound healing. Additionally, we also measured the thickness of the epithelium post 21 days of surgery. The epidermis thickness of the control, CCol-Cl, and CsADM-Cl-treated groups was 97 ± 8.21, 84 ± 10.1, and 59 ± 3.24 μm, respectively (Figure 7e). The epidermal thickness of the CsADM-treated group was much closer to the reported values of the epidermal thickness of NS, that is, 42.0 ± 7.1 μm.[57]

As shown in Figure 8a, collagen deposition and arrangement were visualized and analyzed using MT staining 21 days post-wounding. Augmented deposition of collagen was observed in CCol-Cl- and CsADM-Cl-treated groups when compared to the SHAM group. However, collagen deposition in the dermis was more organized with a basket weave pattern in the CsADM-Cl-treated group. Also, densely packed random collagen fibers were observed in the CCol-Cl-treated group and SHAM group exhibited partial dysplastic collagen fibers. Quantitative image analysis of MT-stained sections revealed acollagen index (intensity of collagen deposition) of 0.42 ± 0.02, 0.74 ± 0.06, and 0.639 ± 0.04 for SHAM, CCol-Cl, and CsADM-Cl, respectively (Figure 8a,b). The collagen index of CsADM-Cl was closest to the collagen index of NS, as reported earlier (*i.e.* 0.601 ± 0.038).[57]

In wound healing, dermal regeneration, re-epithelialization, and formation of the secondary structure play a pivotal role to restore tissue functionality, strength, and aesthetic view.[58] It has been widely reported that cytokines and growth factors are essential for accelerating wound healing, regarding enhanced wound closure and re-epithelialization.[59,60] Therefore, accelerated healing in the CsADM-Cl-treated group can be attributed to embedded native proteins, GAGs, cytokines, growth factors, and also to the unique antibacterial and ROS scavenging activity of the hydrogel variant.

3.16. Immuno Histochemical Analysis. Angiogenesis is a fundamental necessity for rapid wound closure, especially in the case of chronic wounds as blood vessels increase the inflow of oxygen and nutrients to the wound area and henceforth promote healing therein.[61,63] In the present study, angiogenesis through the *in vivo* model was assessed *via* CD31 immunofluorescence staining, as shown in Figure 8c,d. Compared to SHAM, the CCol-Cl treated group showed significantly ($p < 0.05$) a higher number of blood vessels at day 7. Further, the newly formed vessels were distinctly visible on a more organized granulation tissue of the CsADM-Cl-treated group. The angiogenesis induced was significantly higher ($p < 0.001$) when compared to both SHAM and CCol-Cl-treated groups post 7-days of surgery. The higher angiogenic activity of CsADM-Cl may be attributed to the release of bioactive molecules from the hydrogel *in situ*. At day 14, blood vessels were observed to follow an increasing trend in the control-treated group. In contrast, both CCol-Cl- and CsADM-Cl-treated groups showed a decrease in number of vessels. The reason may be the rapid closure of wounds in CCol-Cl- and CsADM-Cl-treated groups. Hence, requirements of blood vessels for the transport of nutrients and oxygen is less, whereas in the SHAM group, healing is still in progress.

Further, to demonstrate re-epithelialization and epidermal differentiation, CK 10 antibody was used for staining 14- and 21-days post-surgery sections (Figure 8e). By day 14, no distinct expression of CK 10 was observed in both SHAM and CCol-Cl-treated groups, revealing the absence of neo-epithelium in the wound area. Surprisingly, the CsADM-Cl-treated group revealed little CK-10 expression in the thick epithelial layer, developing at the interface of the wound. At 21 day post-wounding, the CsADM-Cl-treated group showed a clear, intense expression of CK-10 in the epithelial layer, revealing complete regeneration and resembling of the NS tissue architecture. However, the CCol-Cl-treated group showed that the thick epithelium and expression of CK-10 was mild comparatively, while the in control-treated group, the expression of CK-10 was non-specific.

3.17. RT-PCR Analysis. To evaluate the molecular aspect of healing in different groups, the expression of genes associated with skin wound healing (COL I, COL III, KRT 10, and KRT 14) was assessed, 21 days post-wounding. As shown in Figure 6e,f, there was upregulation in the Col I expression in the CsADM-Cl-treated group when compared to the SHAM/CCol-Cl-treated group. This enhanced expression can be credited to accelerated wound healing observed in the CsADM-Cl-treated group. Interestingly, the downregulation in the expression of Col III, KRT 10, and KRT 14 in the CsADM-Cl-treated group when compared to other group reveals that the re-epithelialization process was more complete and the remodeling phase has started to regain the tissue native strength.

4. DISCUSSION

Bioactive matrices with appropriate physiochemical and biological properties are required to induce rapid wound closure to support cell infiltration, adhesion, and differentiation to regain tissue morphology and function. It has been established in the literature that burn wounds, if healed within 21 days, exhibit minimal scar formation.[64] In the present work, a rapid injectable bioactive hydrogel was developed by dual cross-linking of the sADM. The compositional training allows the hydrogels to preserve their inherent biochemical composition and also lending the gel a unique antioxidant and antibacterial property. Although sADMs from varied origins have been utilized either alone or as a hybrid for tissue engineering, minimal reports are available for an antibacterial sADM-based hydrogel with retained bioactive cues. Our study has utilized DHF-I as a crosslinker for the development of an injectable sADM-based hydrogel with inherent antibacterial property for application in critical burn wounds. Perhaps, this

https://dx.doi.org/10.1021/acs.biomac.0c01400
Biomacromolecules 2021, 22, 514−533

is the first report to utilize DHF-I crosslinker for wound healing study.

In our processing approach, ADM was decellularized using a combinatorial approach, and to lessen surgical trauma due to scaffold implantation in particular, an injectable hydrogel of a decellularized tissue was developed using enzymatic (pepsin) digestion, as reported in the literature.[29] The biggest obstacle for decellularization is to get rid of cellular components (including RNA and DNA) and hence minimizing the immune response, while retaining the inherent bioactive molecules. DAPI and H&E staining of NS and ADM reveal the absence of cells in the ADM; further, DNA quantification supported successful decellularization of the ADM. The DNA content of the ADM (30.14 ± 12.34 ng/mg dry wt) is less than the minimal criterion (50 ng/mg dry wt) required for complete decellularization.[65] To emulate the intricacy of the NS, the ADM must retain multifarious structural and functional proteins, GAGs, glycoproteins, and bioactive cues (growth factors and cytokines), which are the unique features of the NS. Both NS and ADM were observed to have non-significant difference in collagen and GAG contents, and these results were consistent with the literature.[36] Further, SDS-PAGE of NS and ADM revealed the presence of several similar bands of similar intensities revealing the complexity of the ECM which was maintained during the decellularization process. Moreover, ELISA assay showed the presence of TGF-β, VEGF, and BMP-2 in both NS and ADM. TGF-β plays an essential role in cell proliferation and differentiation, immune response, angiogenesis, and tissue repair. It also assists in the production of a new matrix in the graft and promotes graft acceptance.[66,67] BMP2 serves as a chemotactic guide to graft for host cells, induces adipogenesis in soft tissue spaces, and promotes stem cell differentiation.[68] VEGF is reported to induce cell migration and neovascularization in the newly formed tissue.[69]

An ideal skin substitute should mimic the native ECM proteins structurally that provides mechanical support and also biologically active that helps in regulating cellular activities. In native tissue ECM, collagen fibrils exist in a 3D network structure composed of multi-layered nano fibrils (10−500 nm).[70] Our fabricated hybrid hydrogels are 3D networks which are fibrillar owing to phase separation induced by physiological pH and temperature, as demonstrated by SEM (fibril size: 90−120 nm). Interestingly, DHF-I cross-linking did not affect the self-assembly of fiber formation in the hydrogel although the fiber diameter reduced after crosslinking, yet it was not significantly different from the uncrosslinked variant. Also, the triple helix structure of collagen was intact in both CCol-Cl and CsADM-Cl, as demonstrated by FTIR data. CsADM-Cl immunostaining revealed the presence Col I, fibronectin, Col III, VEGF, IL-8, and MCP-1. IL-8 is reported to promote skin re-epithelialization by increasing keratinocyte migration, and MCP-1 has been utilized in the literature to promote dermal wound healing by acting as a chemo attractant for the cells.[71−73] DHF-I crosslinking enhanced the mechanical strength of the hydrogel; crosslinked hydrogels were approximately double in strength when compared to the uncrosslinked variant (as revealed by rheological study).

Wound healing may be hindered by the bacterial load present on the chronic wounds since the high bacterial load present on the wound site delays the wound healing by upregulating the MMP production, which in turn adversely affects collagen deposition and remodeling. To reduce the wound region's bacterial load, the antibacterial skin substitute is required. Herein, we have taken low molecular-weight CTS for the study since it has been reported for its antibacterial property. Further, DHF-I crosslinking synergizes with the polymer's inherent property, and the hybrid is observed to have excellent antibacterial property against *E. coli* and *S. aureus* taken for the study. The antimicrobial activity of iodine has been reported not only against bacteria but also fungi, tubercle bacilli, and viruses; additionally, bacteria does not develop resistance against iodine unlike antibiotics. Iodine is a vital component of the thyroid hormone and hence is biologically safe and can be excreted by the kidneys.[11] The antibacterial property therefore can be attributed to the release of iodine from the crosslinked hybrid hydrogel. It has also been reported in the literature that iodine has antibacterial property owing to its irreversible reaction to tyrosine residues/sites of unsaturation in lipids, oxidation of the sulfhydryl group, and interference in the H-bonding of certain amino acid/nucleic acid.[74] The release of iodine may be due to the instability of the di-iodinated compound in room temperature/light leading to the tendency to revert to iodine and olefin. Iodine, being an acceptor, is able to form complexes with donor compounds. The complex is reported to be weak when formed with ethers, esters, benzene, and ketones using polar solvents, while it forms a strong complex with the amino group-containing compounds like triethylamine/pyridine.[75] However, the exact mechanism of the release of elemental iodine from the hybrid is not established. Thus, antibacterial CsADM-Cl-containing peptides, GAGs, cytokines, and growth factors can act as an apt matrix for facilitating rapid wound closure when compared to CCol-Cl.

Skin mainly consists of fibroblasts and keratinocytes, while stem cells and melanocytes are present in a small number. Fibroblasts or keratinocytes or both have been utilized for the assessment of graft potential as a skin substitute *in vitro*. Hence, both fibroblast and keratinocytes were selected for *in vitro* biological evaluation of the hydrogel. In the present study, conditioning media of the hydrogels revealed the absence of any toxic remnant chemicals, while promoted cell adhesion, migration, and proliferation of cells (HFCs and HKCs). All these cell fate processes are confirmed using a spectrum of assays, including MTT assay, scratch assay, and rhodamine & DAPI staining. The hybrid hydrogel showed uniform viable cellularization on blending the pregel solution and fibroblast cells, that is, as demonstrated by Live/Dead staining post 3 days of encapsulation. Further, no apoptotic cell could be observed in any of the hydrogel posts 7 days seeding, revealing the excellent cytocompatibility of the hydrogels. In addition, cells were observed to be actively proliferating on hydrogel-coated coverslips when stained with PCNA staining. Interestingly, statistically higher ($p < 0.001$) PCNA positive cells were found on CsADM-Cl-coated coverslips. This may be attributed to bioactive molecules in CsADM-Cl.

Angiogenesis is a vital aspect in the wound healing cascade, which governs the initial granulation tissue formation and tissue remodeling.[61,62] Moreover, insufficient vasculature can cause necrosis, ultimately leading to the rejection of the graft. In this context, the angiogenic potential of CsADM-Cl was demonstrated by *ex vivo* CAM assay. The CsADM-Cl hydrogel implant was observed to attract significantly a higher number of allantoic vessels when compared to CCol-Cl hydrogel-implanted CAM. The angiogenic property may be assigned to growth factors (TGF-β and VEGF), preserved during the decellularization and fabrication process. The good injectability

https://dx.doi.org/10.1021/acs.biomac.0c01400
Biomacromolecules 2021, 22, 514−533

of the crosslinked hydrogel was established by injecting the pregel solution into the rat subcutaneous tissue. The qualitative and quantitative outcome of *in vivo* experiments clearly indicated that the new hybrid hydrogel is suitable as an injectable material for minimally invasive surgery. Histological assessment of the hydrogels revealed *in vivo* degradation of the hydrogel and also good attachment of the remnant hydrogel to the host tissue was observed. The degradation of the hydrogel would release many bioactive components, such as peptides, which are useful for recruitment of cell and tissue remodeling, although many components are still unknown. The CsADM-Cl-injected group showed more infiltration of cells when compared to the CCol-Cl-injected group. The cell infiltration into the scaffolds is especially useful for tissue remodeling and regeneration. In addition, no immune cell or capsular protein layer encapsulating the hydrogel was observed in any of the group. Iodine is known for its toxicity, so to ensure non-toxic degradation of the hydrogel, vital organs were harvested and histological evaluation was performed. All the organs showed a similar histological morphology to the control/untreated group, and characteristic morphological features can be easily identified revealing the non-toxic nature of CCol-Cl and CsADM-Cl upon degradation.

The biomedical potential of CCol-Cl and CsADM-Cl to treat chronic wounds was assessed in thermal burn wounds created in a rat model. The ECM from the tissue of origin is the best alternative for regeneration as it contains all proteins, proteoglycans, glycosaminoglycans, cytokines, and growth factors required for the normal functioning of a tissue.[70] Also, the presence of iodine in the hydrogel protected the wound bed from bacterial infection and free-radical load, which otherwise can delay the healing progression therein.[76,77] CsADM-Cl-treated wounds were observed to be rapidly closing with enhanced re-epithelialization when compared to the control- or CCol-Cl-treated group. Moreover, the CsADM-Cl-treated wounds showed the development of more organized/structured collagen deposition, which is much closer to the distribution of collagen in the native tissue. Further, the collagen index of CsADM-Cl-treated wounds was close to the NS as reported in the literature. The presence of proteins, GAGs, cytokines, and growth factors (CK-8, MCP-1, TGF-β, VEGF, and others not quantified) in CsADM-Cl along with a nanoscale fibrillar topology provided ambient biochemical and physiological cues for rapid tissue regeneration. Gene profiling post 21 days for the healing tissue also supported our data. COL I was upregulated in all the group revealing the progression of the healing process, that is, conversion of COL III to COL I, with the expression being strongest in CsADM-Cl. In addition, COL III, KRT 10, and KRT 14 were down-regulated in CsADM-CL, demonstrating more complete tissue regeneration when compared to SHAM/CCol-Cl. Taken together, our study demonstrates that CsADM-Cl hydrogel promoted rapid wound closure, enhanced neovascularization, and complete skin regeneration post 21 days of wounding with superior well-defined dermal−epidermal junctions (DEJ), collagen index native to NS, and skin appendages. Thus, CsADM-Cl hydrogel holds significant potential to serve as a unique graft for superior treatment of dermal wounds in clinical applications.

5. CONCLUSIONS

An injectable hybrid hydrogel CsADM-Cl derived from the rat dermal tissue was developed through modified decellularization, pepsin digestion, and crosslinking. The newly fabricated CsADM-Cl hydrogel successfully retained cytokines and growth factors, which have the potential to guide the tissue regeneration even in chronic conditions. The CsADM-Cl hydrogel exhibited a fibrous morphology and also, gel strength can be tailored by altering crosslinker's concentration. The CsADM-Cl exhibited excellent antibacterial activity against *E. coli* and *S. aureus* and good cytocompatibility with HFCs and HKCs *in vitro*. HFCs were easily encapsulated into the CsADM-Cl hydrogel and proliferated well inside. Importantly, the CsADM-Cl hydrogel allowed a rapid cell infiltration *in vitro* and *in vivo*. It possessed superior angiogenic potential and was observed to be nonimmunogenic without toxicity to major organs studied. Moreover, the CsADM-Cl hydrogel-treated wounds were completely healed with well-defined DEJ and more pronounced secondary appendages. Altogether, our study clearly demonstrates that the CsADM-Cl hydrogel with its nanofibrillar topography, physiochemical composition, antibacterial activity, and injectability can serve as an apt graft for rapid wound healing in chronic wounds.

■ ASSOCIATED CONTENT

Supporting Information

The Supporting Information is available free of charge at https://pubs.acs.org/doi/10.1021/acs.biomac.0c01400.

Histological studies, DNA quantification, SDS PAGE, sGAG assay, collagen quantification, and primer sequences (PDF)

■ AUTHOR INFORMATION

Corresponding Author

Santanu Dhara − *Biomaterials and Tissue Engineering Laboratory, School of Medical Science and Technology, Indian Institute of Technology Kharagpur, Kharagpur 721302, India;* orcid.org/0000-0003-4443-7610; Email: sdhara@smst.iitkgp.ernet.in

Authors

Kamakshi Bankoti − *Biomaterials and Tissue Engineering Laboratory, School of Medical Science and Technology, Indian Institute of Technology Kharagpur, Kharagpur 721302, India*

Arun Prabhu Rameshbabu − *Biomaterials and Tissue Engineering Laboratory, School of Medical Science and Technology, Indian Institute of Technology Kharagpur, Kharagpur 721302, India*

Sayanti Datta − *Biomaterials and Tissue Engineering Laboratory, School of Medical Science and Technology, Indian Institute of Technology Kharagpur, Kharagpur 721302, India*

Piyali Goswami − *Department of Biotechnology, Indian Institute of Technology Kharagpur, Kharagpur 721302, India*

Madhurima Roy − *Department of Biotechnology, Indian Institute of Technology Kharagpur, Kharagpur 721302, India*

Dipankar Das − *Polymer Chemistry Laboratory, Department of Applied Chemistry, Indian Institute of Technology (Indian School of Mines), Dhanbad 826004, India;* orcid.org/0000-0001-9298-6871

https://dx.doi.org/10.1021/acs.biomac.0c01400
Biomacromolecules 2021, 22, 514−533

Sudip Kumar Ghosh − *Department of Biotechnology, Indian Institute of Technology Kharagpur, Kharagpur 721302, India*
Amit Kumar Das − *Department of Biotechnology, Indian Institute of Technology Kharagpur, Kharagpur 721302, India*
Analava Mitra − *Natural Products Research Laboratory, School of Medical Science and Technology, Indian Institute of Technology Kharagpur, Kharagpur 721302, India;* orcid.org/0000-0003-2597-0794
Sagar Pal − *Polymer Chemistry Laboratory, Department of Applied Chemistry, Indian Institute of Technology (Indian School of Mines), Dhanbad 826004, India;* orcid.org/0000-0002-3425-7010
Dhrubajyoti Maulik − *Department of Surgery, Bankura Sammilani Medical College, Bankura 722102, India*
Bo Su − *Bristol Dental School, University of Bristol, Bristol BS1 2LY, U.K.*
Paulomi Ghosh − *Structural Biology and Bioinformatics, CSIR-Indian Institute of Chemical Biology (CSIR-IICB), Kolkata 700032, India*
Bikramajit Basu − *Materials Research Center, Indian Institute of Science, Bangalore 560012, India*

Complete contact information is available at: https://pubs.acs.org/10.1021/acs.biomac.0c01400

Notes

The authors declare no competing financial interest.

■ ACKNOWLEDGMENTS

Authors acknowledge fellowship received from Department of Science and Technology (DST, Govt. of India) for K.B. and Ministry of Human Resource Development (MHRD, Govt. of India) for S.D. and A.P.R. Nantu Dogra is acknowledged for helping in laboratory experiments. Project (BT/PR7818/MED/32/279/2013) funding from the Department of Biotechnology is acknowledged.

■ REFERENCES

(1) Loo, Y.; Wong, Y.-C.; Cai, E. Z.; Ang, C.-H.; Raju, A.; Lakshmanan, A.; Koh, A. G.; Zhou, H. J.; Lim, T.-C.; Moochhala, S. M.; Hauser, C. A. E. Ultrashort Peptide Nanofibrous Hydrogels for the Acceleration of Healing of Burn Wounds. *Biomaterials* **2014**, *35*, 4805−4814.
(2) Selig, H. F.; Lumenta, D. B.; Giretzlehner, M.; Jeschke, M. G.; Upton, D.; Kamolz, L. P. The Properties of an "Ideal" Burn Wound Dressing − What Do We Need in Daily Clinical Practice? Results of A Worldwide Online Survey Among Burn Care Specialists. *Burns* **2012**, *38*, 960−966.
(3) Ravishanker, R.; Bath, A. S.; Roy, R. Amnion Bank-The Use of Long-Term Glycerol Preserved Amniotic Membranes in the Management of Superficial and Superficial Partial-Thickness Burns. *Burns* **2003**, *29*, 369−374.
(4) Gist, S.; Iris, T. M.; Falzgraf, S.; Cameron, S.; Beebe, M. Wound Care in the Geriatric Client. *Clin. Interv. Aging* **2009**, *4*, 269−287.
(5) Okan, D.; Woo, K.; Ayello, E. A.; Sibbald, G. The Role of Moisture Balance in Wound Healing. *Adv. Skin Wound Care* **2007**, *20*, 39−53.
(6) Hrynyk, M.; Martins-Green, M.; Barron, A. E.; Neufeld, R. J. Alginate-PEG Sponge Architecture and Role in The Design of Insulin Release Dressings. *Biomacromolecules* **2012**, *13*, 1478−1485.
(7) Liu, Y.; Petreaca, M.; Martins-Green, M. Cell and Molecular Mechanisms of Insulin-Induced Angiogenesis. *J. Cell Mol. Med.* **2009**, *13*, 4492−4504.
(8) Ito, T.; Fraser, I. P.; Yeo, Y.; Highley, C. B.; Bellas, E.; Kohane, D. S. Anti-Inflammatory Function of an In Situ Cross-Linkable Conjugate Hydrogel of Hyaluronic Acid and Dexamethasone. *Biomaterials* **2007**, *28*, 1778−1786.
(9) Salick, D. A.; Kretsinger, J. K.; Pochan, D. J.; Schneider, J. P. Inherent Antibacterial Activity of a Peptide-Based Beta-Hairpin Hydrogel. *J. Am. Chem. Soc.* **2007**, *129*, 14793−14799.
(10) McDonnell, G.; Russell, A. D. Antiseptics and Disinfectants: Activity, Action, and Resistance. *Clin. Microbiol. Rev.* **1999**, *12*, 147−179.
(11) Shirai, T.; Shimizu, T.; Ohtani, K.; Zen, Y.; Takaya, M.; Tsuchiya, H. Antibacterial Iodine-Supported Titanium Implants. *Acta Biomater.* **2011**, *7*, 1928−1933.
(12) Durani, P.; Leaper, D. Povidone−Iodine: Use in Hand Disinfection, Skin Preparation and Antiseptic Irrigation. *Int. Wound J.* **2008**, *5*, 376−387.
(13) Ong, S.-Y.; Wu, J.; Moochhala, S. M.; Tan, M.-H.; Lu, J. Development of a Chitosan-Based Wound Dressing with Improved Hemostatic and Antibacterial Properties. *Biomaterials* **2008**, *29*, 4323−4332.
(14) Kim, I.-Y.; Seo, S.-J.; Moon, H.-S.; Yoo, M.-K.; Park, I.-Y.; Kim, B.-C.; Cho, C.-S. Chitosan and its Derivatives for Tissue Engineering Applications. *Biotechnol. Adv.* **2008**, *26*, 1−21.
(15) Sana, F. A.; Yurtsever, M. C.; Bayrak, G. K.; Tuncay, E. O.; Kiremitci, A. S.; Gumusderelioglu, M. Spreading, Proliferation and Differentiation of Human Dental Pulp Stem Cells on Chitosan Scaffolds Immobilized with RGD or Fibronectin. *Cytotechnology* **2017**, *69*, 617−630.
(16) Liu, H.; Fan, H.; Cui, Y.; Chen, Y.; Yao, K.; Goh, J. C. H. Effects of The Controlled-Released Basic Fibroblast Growth Factor from Chitosan−Gelatin Microspheres on Human Fibroblasts Cultured on A Chitosan−Gelatin Scaffold. *Biomacromolecules* **2007**, *8*, 1446−1455.
(17) Ikemoto, S.; Mochizuki, M.; Yamada, M.; Takeda, A.; Uchinuma, E.; Yamashina, S.; Nomizu, M.; Kadoya, Y. Laminin Peptide-Conjugated Chitosan Membrane: Application for Keratinocyte Delivery in Wounded Skin. *J. Biomed. Mater. Res., Part A* **2006**, *79*, 716−722.
(18) Hozumi, K.; Yamagata, N.; Otagiri, D.; Fujimori, C.; Kikkawa, Y.; Kadoya, Y.; Nomizu, M. Mixed Peptide−Chitosan Membranes to Mimic the Biological Activities of a Multifunctional Laminin A1 Chain LG4 Module. *Biomaterials* **2009**, *30*, 1596−1603.
(19) Ma, L.; Gao, C.; Mao, Z.; Zhou, J.; Shen, J.; Hu, X.; Han, C. Collagen/Chitosan Porous Scaffolds with Improved Biostability For Skin Tissue Engineering. *Biomaterials* **2003**, *24*, 4833−4841.
(20) Ueno, H.; Mori, T.; Fujinaga, T. Topical Formulations and Wound Healing Applications of Chitosan. *Adv. Drug Delivery Rev.* **2001**, *52*, 105−115.
(21) Lecht, S.; Stabler, C. T.; Rylander, A. L.; Chiaverelli, R.; Schulman, E. S.; Marcinkiewicz, C.; Lelkes, P. I. Enhanced Reseeding of Decellularized Rodent Lungs with Mouse Embryonic Stem Cells. *Biomaterials* **2014**, *35*, 3252−3262.
(22) Watt, F. M.; Huck, W. T. S. Role of The Extracellular Matrix in Regulating Stem Cell Fate. *Nat. Rev. Mol. Cell Biol.* **2013**, *14*, 467−473.
(23) Clause, K. C.; Barker, T. H. Extracellular Matrix Signaling in Morphogenesis and Repair. *Curr. Opin. Biotechnol.* **2013**, *24*, 830−833.
(24) Reing, J. E.; Zhang, L.; Myers-Irvin, J.; Cordero, K. E.; Freytes, D. O.; Heber-Katz, E.; Bedelbaeva, K.; McIntosh, D.; Dewilde, A.; Braunhut, S. J.; Badylak, S. F. Degradation Products of Extracellular Matrix Affect Cell Migration and Proliferation. *Tissue Eng., Part A* **2009**, *15*, 605−614.
(25) Brennan, E. P.; Tang, X.-H.; Stewart-Akers, A. M.; Gudas, L. J.; Badylak, S. F. Chemoattractant Activity of Degradation Products of Fetal and Adult Skin Extracellular Matrix for Keratinocyte Progenitor Cells. *J. Tissue Eng. Regener. Med.* **2008**, *2*, 491−498.
(26) Yang, Q.; Peng, J.; Guo, Q.; Huang, J.; Zhang, L.; Yao, J.; Yang, F.; Wang, S.; Xu, W.; Wang, A.; Lu, S. A Cartilage ECM-Derived 3-D

Porous Acellular Matrix Scaffold For In Vivo Cartilage Tissue Engineering With PKH26-Labeled Chondrogenic Bone Marrow-Derived Mesenchymal Stem Cells. *Biomaterials* **2008**, *29*, 2378−2387.
(27) Gilbert, T.; Sellaro, T. L.; Badylak, S. F. Decellularization of tissues and organs. *Biomaterials* **2006**, *27*, 3675−3683.
(28) Lee, J. S.; Shin, J.; Park, H.-M.; Kim, Y.-G.; Kim, B.-G.; Oh, J.-W.; Cho, S.-W. Liver Extracellular Matrix Providing Dual Functions of Two-Dimensional Substrate Coating and Three-Dimensional Injectable Hydrogel Platform for Liver Tissue Engineering. *Biomacromolecules* **2014**, *15*, 206−218.
(29) Wolf, M. T.; Daly, K. A.; Brennan-Pierce, E. P.; Johnson, S. A.; Carruthers, C. A.; D'Amore, A.; Nagarkar, S. P.; Velankar, S. S.; Badylak, S. F. A Hydrogel Derived from Decellularized Dermal Extracellular Matrix. *Biomaterials* **2012**, *33*, 7028−7038.
(30) Young, B. M.; Shankar, K.; Allen, B. P.; Pouliot, R. A.; Schneck, M. B.; Mikhaiel, N. S.; Heise, R. L. Electrospun decellularized lung matrix scaffold for airway smooth muscle culture. *ACS Biomater. Sci. Eng.* **2017**, *3*, 3480−3492.
(31) Efraim, Y.; Sarig, H.; Cohen Anavy, N.; Sarig, U.; de Berardinis, E.; Chaw, S.-Y.; Krishnamoorthi, M.; Kalifa, J.; Bogireddi, H.; Duc, T. V.; Kofidis, T.; Baruch, L.; Boey, F. Y. C.; Venkatraman, S. S.; Machluf, M. Biohybrid Cardiac ECM-Based Hydrogels Improve Long Term Cardiac Function Post Myocardial Infarction. *Acta Biomater.* **2017**, *50*, 220−233.
(32) Gupta, V.; Lyne, D. V.; Laflin, A. D.; Zabel, T. A.; Barragan, M.; Bunch, J. T.; Pacicca, D. M.; Detamore, M. S. Microsphere-Based Osteochondral Scaffolds Carrying Opposing Gradients of Decellularized Cartilage and Demineralized Bone Matrix. *ACS Biomater. Sci. Eng.* **2017**, *3*, 1955−1963.
(33) Rameshbabu, A. P.; Bankoti, K.; Datta, S.; Subramani, E.; Apoorva, A.; Ghosh, P.; Maity, P. P.; Manchikanti, P.; Chaudhury, K.; Dhara, S. Silk Sponges Ornamented With A Placenta-Derived Extracellular Matrix Augment Full-Thickness Cutaneous Wound Healing By Stimulating Neovascularization And Cellular Migration. *ACS Appl. Mater. Interfaces* **2018**, *10*, 16977−16991.
(34) Qiu, J.; Jianhua, L.; Guancong, W.; Lin, Z.; Na, R.; Hong, L.; Wei, T.; Huaidong, J.; Yingjun, W. In Vitro Investigation on The Biodegradability And Biocompatibility Of Genipin Cross-Linked Porcine Acellular Dermal Matrix With Intrinsic Fluorescence. *ACS Appl. Mater. Interfaces* **2013**, *5*, 344−350.
(35) Kumar, N.; Gangwar, A. K.; Sharma, A. K.; Negi, M.; Shrivastava, S.; Mathew, D. D.; Sonal, V. R.; Maiti, S. K.; Devi, K. S.; Kumar, V.; Ramteke, P. W.; Kaarthick, D. T.; Kurade, N. P. Extraction Techniques for The Decellularization of Rat Dermal Constructs. *Trends Biomater. Artif. Organs* **2013**, *27*, 102−107.
(36) Reing, J. E.; Brown, B. N.; Daly, K. A.; Freund, J. M.; Gilbert, T. W.; Hsiong, S. X.; Huber, A.; Kullas, K. E.; Tottey, S.; Wolf, M. T.; Badylak, S. F. The Effects of Processing Methods Upon Mechanical and Biologic Properties of Porcine Dermal Extracellular Matrix Scaffolds. *Biomaterials* **2010**, *31*, 8626−8633.
(37) Rajan, N.; Habermehl, J.; Coté, M.-F.; Doillon, C. J.; Mantovani, D. Preparation of Ready-To-Use, Storable and Reconstituted Type I Collagen from Rat Tail Tendon for Tissue Engineering Applications. *Nat. Protoc.* **2006**, *1*, 2753−2758.
(38) Ghosh, P.; Das, M.; Rameshbabu, A. P.; Das, D.; Datta, S.; Pal, S.; Panda, A. B.; Dhara, S. Chitosan Derivatives Cross-Linked with Iodinated 2,5-Dimethoxy-2,5- Dihydrofuran for Non-Invasive Imaging. *ACS Appl. Mater. Interfaces* **2014**, *6*, 17926−17936.
(39) Zhao, X.; Wu, H.; Guo, B.; Dong, R.; Qiu, Y.; Ma, P. X. Antibacterial Anti-Oxidant Electroactive Injectable Hydrogel as Self-Healing Wound Dressing with Hemostasis and Adhesiveness For Cutaneous Wound Healing. *Biomaterials* **2017**, *122*, 34−47.
(40) Punnakitikashem, P.; Truong, D.; Menon, J. U.; Nguyen, K. T.; Hong, Y. Electrospun Biodegradable Elastic Polyurethane Scaffolds with Dipyridamole Release for Small Diameter Vascular Grafts. *Acta Biomater.* **2014**, *10*, 4618−4628.
(41) Li, P.; Poon, Y. F.; Li, W.; Zhu, H.-Y.; Yeap, S. H.; Cao, Y.; Qi, X.; Zhou, C.; Lamrani, M.; Beuerman, R. W.; Kang, E.-T.; Mu, Y.; Li, C. M.; Chang, M. W.; Jan Leong, S. S.; Chan-Park, M. B. A Polycationic Antimicrobial and Biocompatible Hydrogel with Microbe Membrane Suctioning. Ability. *Nat. Mater.* **2010**, *10*, 149−156.
(42) Aasen, T.; Belmonte, J. C. I. Isolation and Cultivation of Human Keratinocytes from Skin or Plucked Hair for The Generation of Induced Pluripotent Stem Cells. *Nat. Protoc.* **2010**, *5*, 371−382.
(43) Sun, G.; Zhang, X.; Shen, Y.-I.; Sebastian, R.; Dickinson, L. E.; Fox-Talbot, K.; Reinblatt, M.; Steenbergen, C.; Harmon, J. W.; Gerecht, S. Dextran Hydrogel Scaffolds Enhance Angiogenic Responses and Promote Complete Skin Regeneration During Burn Wound Healing. *Proc. Natl. Acad. Sci. U.S.A.* **2011**, *108*, 20976−20981.
(44) Terzi, A.; Storelli, E.; Bettini, S.; Sibillano, T.; Altamura, L.; Salvatore, M.; Madaghiele, A.; Romano, D.; Siliqi, M.; Ladisa, L.; De Caro, A.; Quattrini, L.; Valli, A.; Sannino, C. G. Effects of Processing on Structural, Mechanical and Biological Properties of Collagen-Based Substrates for Regenerative Medicine. *Sci. Rep.* **2018**, *8*, 1429.
(45) Fernandes, L. L.; Resende, C. X.; Tavares, D. S.; Soares, G. A.; Castro, L. O.; Granjeiro, J. M. Cytocompatibility of Chitosan and Collagen-Chitosan Scaffolds for Tissue Engineering. *Polimeros* **2011**, *21*, 1−6.
(46) Huang, Y.; Wang, Y.; Chen, L.; Zhang, L. Facile Construction of Mechanically Tough Collagen Fibers Reinforced by Chitin Nanofibers as Cell Alignment Templates. *J. Mater. Chem. B* **2018**, *6*, 918−929.
(47) Sen, C. K.; Khanna, S.; Gordillo, G.; Bagchi, D.; Bagchi, M.; Roy, S. Oxygen, Oxidants, and Antioxidants in Wound Healing. *Ann. N.Y. Acad. Sci.* **2002**, *957*, 239−249.
(48) Aceves, C.; Anguiano, B.; Delgado, G. The Extrathyronine Actions of Iodine as Antioxidant, Apoptotic, and Differentiation Factor in Various Tissues. *Thyroid* **2013**, *23*, 938−946.
(49) Jaganathan, S.; Balaji, A.; Ismail, A. F.; Rajasekar, R. Fabrication and Hemocompatibility Assessment of Novel Polyurethane-Based Bio-Nanofibrous Dressing Loaded with Honey and Carica Papaya Extract for The Management of Burn Injuries. *Int. J. Nanomed.* **2016**, *11*, 4339−4355.
(50) ASTM. Hemocompatibility results Document ASTM. Standard Practice for Assessment of Hemolytic Properties of Materials Designation: F 756-00. *Annual Book of ASTM Standards*, 2005; pp 309−313.
(51) Church, D.; Elsayed, S.; Reid, O.; Winston, B.; Lindsay, R. Burn Wound Infections. *Clin. Microbiol. Rev.* **2006**, *19*, 403−434.
(52) Zubko, E. I.; Zubko, M. K. Co-Operative Inhibitory Effects of Hydrogen Peroxide and Iodine Against Bacterial and Yeast Species. *BMC Res. Notes* **2013**, *6*, 272−279.
(53) Punyani, S.; Narayanan, P.; Vasudevan, P.; Singh, H. Sustained Release of Iodine from a Polymeric Hydrogel Device for Water Disinfection. *J. Appl. Polym. Sci.* **2007**, *103*, 3334−3340.
(54) Raghow, R. The Role of Extracellular Matrix in Post Inflammatory Wound Healing and Fibrosis. *FASEB J.* **1994**, *8*, 823−831.
(55) Lawrence, W. T.; Diegelmann, R. F. Growth Factors in Wound Healing. *Clin. Dermatol.* **1994**, *12*, 157−169.
(56) Greenwel, P.; Inagaki, Y.; Hu, W.; Walsh, M.; Ramirez, F. Sp1 is Required for the Early Response of A2 (I) Collagen to Transforming Growth Factor-β1. *J. Biol. Chem.* **1997**, *272*, 19738−19745.
(57) Li, Z.; Zhou, F.; Li, Z.; Lin, S.; Chen, L.; Liu, L.; Chen, Y. Hydrogel Cross-Linked with Dynamic Covalent Bonding and Micellization for Promoting Burn Wound Healing. *ACS Appl. Mater. Interfaces* **2018**, *10*, 25194−25202.
(58) Metcalfe, A. D.; Ferguson, M. W. J. Tissue Engineering of Replacement Skin: The Crossroads of Biomaterials, Wound Healing, Embryonic Development, Stem Cells and Regeneration. *J. R. Soc. Interface* **2007**, *4*, 413−437.
(59) Rameshbabu, A. P.; Bankoti, K.; Datta, S.; Subramani, E.; Apoorva, A.; Ghosh, P.; Maity, P. P.; Manchikanti, P.; Chaudhury, K.; Dhara, S. Silk Sponges Ornamented with a Placenta-Derived Extracellular Matrix Augment Full-Thickness Cutaneous Wound

https://dx.doi.org/10.1021/acs.biomac.0c01400
Biomacromolecules 2021, 22, 514−533

Healing by Stimulating Neovascularization and Cellular Migration. *ACS Appl. Mater. Interfaces* **2018**, *10*, 16977−16991.
(60) Choi, J. U.; Lee, S. W.; Pangeni, R.; Byun, Y.; Yoon, I.-S.; Park, J. W. Preparation and In Vivo Evaluation of Cationic Elastic Liposomes Comprising Highly Skin-Permeable Growth Factors Combined with Hyaluronic Acid for Enhanced Diabetic Wound-Healing Therapy. *Acta Biomater.* **2017**, *57*, 197−215.
(61) Madeddu, P. Therapeutic Angiogenesis and Vasculogenesis for Tissue Regeneration. *Exp. Physiol.* **2005**, *90*, 315−326.
(62) Nomi, M.; Atala, A.; Coppi, P. D.; Soker, S. Principals of Neovascularization for Tissue Engineering. *Mol. Aspect. Med.* **2002**, *23*, 463−483.
(63) Tan, Q.; Chen, B.; Yan, X.; Lin, Y.; Xiao, Z.; Hou, X.; Dai, J. Promotion of Diabetic Wound Healing by Collagen Scaffold with Collagen Binding Vascular Endothelial Growth Factor in A Diabetic Rat Model. *J. Tissue Eng. Regener. Med.* **2014**, *8*, 195−201.
(64) Sun, G.; Zhang, X.; Shen, Y.-I.; Sebastian, R.; Dickinson, L. E.; Fox-Talbot, K.; Reinblatt, M.; Steenbergen, C.; Harmon, J. W.; Gerecht, S. Dextran Hydrogel Scaffolds Enhance Angiogenic Responses and Promote Complete Skin Regeneration During Burn Wound Healing. *Proc. Natl. Acad. Sci. U.S.A.* **2011**, *108*, 20976−20981.
(65) Crapo, P. M.; Gilbert, T. W.; Badylak, S. F. An Overview of Tissue and Whole Organ Decellularization Processes. *Biomaterials* **2011**, *32*, 3233−3243.
(66) Penn, J. W.; Grobbelaar, A. O.; Rolfe, K. J. The Role of the TGF-B Family in Wound Healing, Burns and Scarring: A Review. *Int. J. Burns Trauma* **2012**, *2*, 18−28.
(67) Pakyari, M.; Farrokhi, A.; Maharlooei, M. K.; Ghahary, A. Critical Role of Transforming Growth Factor Beta in Different Phases of Wound Healing. *Adv. Wound Care* **2013**, *2*, 215−224.
(68) Sottile, V.; Seuwen, K. Bone Morphogenetic Protein-2 Stimulates Adipogenic Differentiation of Mesenchymal Precursor Cells in Synergy with BRL 49653 (Rosiglitazone). *FEBS Lett.* **2000**, *475*, 201−204.
(69) Johnson, K. E.; Wilgus, T. A. Vascular Endothelial Growth Factor and Angiogenesis in the Regulation of Cutaneous Wound Repair. *Adv. Wound Care* **2014**, *3*, 647−661.
(70) Mouw, J. K.; Ou, G.; Weaver, V. M. Extracellular Matrix Assembly: A Multiscale Deconstruction. *Nat. Rev. Mol. Cell Biol.* **2014**, *15*, 771−785.
(71) Engelhardt, E.; Toksoy, A.; Goebeler, M.; Debus, S.; Bröcker, E.-B.; Gillitzer, R. Chemokines IL-8, Groalpha, MCP-1, IP-10, And Mig are Sequentially and Differentially Expressed During Phase-Specific Infiltration of Leukocyte Subsets in Human Wound Healing. *Am. J. Pathol.* **1998**, *153*, 1849−1860.
(72) Rennekampff, H.-O.; Hansbrough, J. F.; Kiessig, V.; Doré, C.; Sticherling, M.; Schröder, J.-M. Bioactive Interleukin-8 Is Expressed in Wounds and Enhances Wound Healing. *J. Surg. Res.* **2000**, *93*, 41−54.
(73) Wood, S.; Jayaraman, V.; Huelsmann, E. J.; Bonish, B.; Burgad, D.; Sivaramakrishnan, G.; Qin, S.; DiPietro, L. A.; Zloza, A.; Zhang, C.; Shafikhani, S. H. Pro-Inflammatory Chemokine Ccl2 (Mcp-1) Promotes Healing in Diabetic Wounds by Restoring the Macrophage Response. *PLoS One* **2014**, *9*, No. e91574.
(74) Some, S.; Sohn, J. S.; Kim, J.; Su-Hyun Lee, S. C.; Lee, J.; Lee, I.; Shackery, S. K.; Kim, S. H.; Kim, N.; Choi, I.; Jung, H.; Kang, S.; Jun, S. C. Graphene-Iodine Nanocomposites: Highly Potent Bacterial Inhibitors that are Bio-Compatible with Human Cells. *Sci. Rep.* **2016**, *6*, 2015.
(75) Lacroix-Desmazes, P.; Severac, R.; Boutevin, B. Reverse Iodine Transfer Polymerization of Methyl Acrylate and N-Butyl Acrylate. *Macromolecules* **2005**, *38*, 6299−6309.
(76) Zhao, D.; Lim, C.-P.; Miyanaga, K.; Tanji, Y. Iodine from Bacterial Iodide Oxidization by Roseovarius Spp. Inhibits the Growth of other Bacteria. *Appl. Microbiol. Biotechnol.* **2012**, *97*, 2173−2182.
(77) Beukelman, C. J.; van den Berg, A. J. J.; Hoekstra, M. J.; Uhl, R.; Reimer, K.; Mueller, S. Anti-Inflammatory Properties of a Liposomal Hydrogel with Povidone-Iodine (Repithel) for Wound Healing In Vitro. *Burns* **2008**, *34*, 845−855.

https://dx.doi.org/10.1021/acs.biomac.0c01400
Biomacromolecules 2021, 22, 514−533